The synergy between osmotically assisted reverse osmosis (OARO) and the use of thermo-responsive draw solutions for energy efficient, zero-liquid discharge desalination

Christian D. Peters[1] and Nicholas P. Hankins[1]

[1]Department of Engineering Science, The University of Oxford, Parks Road, OX3 1PJ, Oxford, UK

June 11, 2020

Abstract

Conventional zero-liquid discharge (ZLD) processes alleviate environmental concerns associated with brine discharge, but are not widely applied, due to their high cost and significant energy consumption. However, new and promising ZLD technologies, such as those integrated with osmotically assisted reverse osmosis (OARO), may be technically and economically more favourable than existing technologies.

In this study, a numerical comparison between an FO and an OARO integrated ZLD process is performed, in which a thermo-responsive draw solution is utilised for both. The findings from the parametric and techno-economic analysis indicate that OARO mitigates several shortcomings of FO, making it more energy efficient (energy savings of $\approx 10.8\,\%$), less susceptible to internal concentration polarisation and more economical (cost savings of $\approx 15.5\,\%$). Furthermore, a key advantage of OARO is that it operates with lower draw solute concentrations allowing for the draw solute to be regenerated at temperatures $12^{\circ}\,C$ lower than with FO operation. This means that low-grade waste heat (LGWH), which is essentially 'free energy', is more easily utilised as an energy source.

In comparison to other hydraulic pressure-driven ZLD technologies, such as low-salt-rejection RO (LSRRO), the electrical energy consumption of OARO can be significantly offset when powered by LGWH and using a thermo-responsive draw solute. The specific electrical energy consumption can be as low as $3.47\,kWh/m^3$ when concentrating a saline stream from 0.6M to 4M using 4 membrane stages. At the same time, a 4-stage LSRRO system would consume approximately 48% more electricity to achieve the same concentration factor. Furthermore, OARO processes operating with a thermo-responsive draw solution can outperform those using non-responsive draw solutes (i.e. NaCl). Brine concentrations of up to $245\,g/kg$ can be achieved using technically feasible operating pressures and draw solute concentrations, while the number of required membrane stages is almost halved from 6 to 4.

1 Introduction

On a worldwide level, desalination technologies produce more than 140 million m^3/day of brine. This is almost 50 % greater than the amount of freshwater they produce (95 million m^3/day) (Jones et al. 2019). Brine is an unwanted desalination by-product that is most economically disposed of by discharging it back into the environment in its untreated state (Arnal et al. 2005). However, untreated brine is often severely polluted and can contain contaminants, such as anti-fouling and anti-scaling additives, anti-foaming additives, oxygen scavengers and corrosion products (Alameddine & El-Fadel 2007). Furthermore, brine is also highly saline and can be discharged at elevated temperatures from thermal desalination processes. Thus, brine in its untreated state can cause severe damage to ocean life and marine ecosystems (Missimer & Maliva 2018, Miller et al. 2015, Roberts et al. 2010).

These negative ecological effects can be circumvented by developing more economically viable and environmentally sound brine management solutions. According to Morillo et al. (2014), brine management solutions can be utilised for (1) brine volume minimisation (BVM), (2) salt and metal recovery, and (3) brine adaption for industry. Salt and metal recovery processes utilise the brine to produce valuable by-products. As stated by Loganathan et al. (2017), the potential exists to extract minerals, such as sodium, magnesium, calcium and bromide, from seawater in an economically favourable manner. Another possibility is to valorise the brine stream by concentrating and adapting it for the chlor-alkali industry and acid-base production (Reig et al. 2014, Casas et al. 2012). Although BVM may not appear to offer any direct economic value, as no additional by-products are produced, higher process recoveries do lead to an exponential decrease in the final brine volume and the required seawater extraction rate (feed) for a constant freshwater production rate. This trend is depicted in figure 1. Lower brine volumes simplify brine disposal and minimise the associated costs; lower feed volumes can reduce pre-treatment costs (Jones et al. 2019).

However, BVM and ultimately zero-liquid discharge (ZLD) processes are not widespread, due to the availability of other more economically viable brine dis-

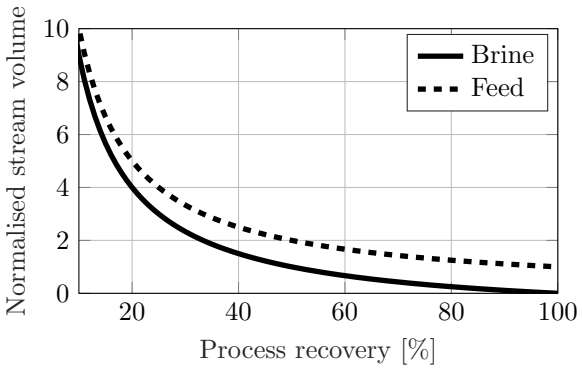

Figure 1: Brine and feed volume with respect to the freshwater recovery of the desalination plant with a constant permeate production rate of 1.

posal options (Tong & Elimelech 2016). Currently, thermal processes, such as mechanical vapor compression (MVC), are the prevailing techniques to dewater brines with a TDS content exceeding 70 g/L to final brine salinities of approximately 250 g/L (Davenport et al. 2018). High capital costs and energy consumption are associated with these thermal processes (e.g. MVC: 7 kWh/m^3 to 25 kWh/m^3; brine concentrator: 18 kWh/m^3 to 26 kWh/m^3 (Tong & Elimelech 2016)), which limits their widespread application. Furthermore, concentrating the brine stream above its solubility limit and crystallising it using thermal-based technologies (if not performed using solar evaporation), proves to be even more capital and energy intensive (e.g. brine crystalliser: 52 kWh/m^3 to 66 kWh/m^3). Solar evaporation has its own deficiencies, such as being limited to dry and warm regions and requiring large amounts of land (Subramani & Jacangelo 2014).

For lower feed salinities (TDS $< 75\,g/L$), membrane-based technologies hold the highest market share in desalination. RO, the most well-known of these technologies, revolutionised the desalination market and is now widely commercialised as the chosen low-energy method. Yet, RO is limited by its maximum operating pressure (Bartholomew et al. 2017). Other membrane-based processes, such as membrane distillation (MD) and crystallisation (MCr) (Sanmartino et al. 2017, Mericq et al. 2010, Ruiz Salmón & Luis 2018), multi-stage reverse osmosis (MSRO), high pressure reverse osmosis (HPRO) (Davenport et al. 2018), low-salt-rejection RO (LSRRO) (Wang et al. 2020), osmotically assisted reverse osmosis (OARO) (Peters & Hankins 2019, Bouma & Lienhard 2018) and forward osmosis (FO) (Shaffer et al. 2015) can be utilised to further dewater the RO concentrate and are thus promising BVM technologies. Electrodialysis and capacitive deionization can also be utilised in BVM processes (Tsai et al. 2017), although they are mainly applied for low salinity feeds. This is due to their relatively high capital and operational expenses and their lower selectivity in comparison to RO (Qin et al. 2019, Campione et al. 2018).

The focus of this article is on osmotically driven membrane processes, as these are promising alternatives to be incorporated into BVM/ZLD processes. For example, FO is hailed by several researchers as having a low fouling propensity or having a high fouling reversibility (Wang 2016, Lotfi et al. 2017, Lee et al. 2017, Cai & Hu 2016). It offers multi-barrier protection against feedwater contaminants for in-series membrane processes (Nguyen et al. 2019), and allows the possibility of regenerating responsive DS using forms of low-grade energy which are cheaper and more renewable than grid-sourced electricity (Johnson et al. 2018, Cai & Hu 2016, Cai et al. 2015).

In spite of these advantages, recent studies (such as that by Wang et al. (2020)) have highlighted the disadvantages of osmotically driven membrane processes, especially those of OARO. One such disadvantage of OARO (and also FO) is that the design of the membrane module and its operation is more complex in comparison to that of purely pressure-driven processes. In addition, internal concentration polarisation (ICP) can have deleterious effects on the performance of all osmotically driven processes and hence membranes with a porous, non-tortuous and thin support layer (small S-value) are required to minimise this phenomenon. Membranes with such substrate specifications suffer from a lower mechanical strength; thus high pressure operation, as required in OARO, may inevitably lead to their failure. While these technical issues remain to be solved, FO and specifically OARO have the potential to significantly reduce the overall energy consumption of BVM and ZLD processes. For example, Bouma & Lienhard (2018) could concentrate a feed stream from 0.6M to 4M using only 3.9 kWh/m^3 whereas a 3-stage and 4-stage LSRRO system with similar operating conditions consumed 9.11 kWh/m^3 and 5.14 kWh/m^3, respectively (Wang et al. 2020).

1.1 Research objectives

In this study, the standard OARO process, which utilises a non-responsive draw solute (i.e. NaCl), is expanded to incorporate thermo-responsive draw solutes to investigate whether this novel combination can outperform 1) a forward osmosis process utilising the same draw solution, 2) the standard OARO process with non-responsive draw solutes, and 3) the LSRRO process.

Although both FO and OARO are promising BVM technologies, there is currently no literature available on a direct comparison (experimental or numerical) of these two technologies. Thus, the first research objective addressed in this article is to investigate whether OARO or FO is the preferable BVM technology. To address this question, a direct parametric and techno-economic comparison is performed. A single test case is chosen here that is based on the membrane brine concentrator (MBC), which forms part of the world's first-ever commercial FO ZLD process (Pendergast et al. 2016). This test scenario is chosen, due to its industrial applicability and due to the possibility of directly comparing the FO and OARO process while using the

same feed conditions, the same draw solution (to exclude any variability caused by the choice of the draw solution (DS) on the results), the same process layout and the same target brine concentration. Therefore, the feed hydraulic pressure is the only variable for which its inclusion can alleviate several of the FO shortcomings. Following this detailed comparison, both the FO and OARO MBC are compared with the LSRRO and the standard OARO process to draw attention to the advantages and possibilities arising when combining OARO with responsive draw solutions.

2 Methodology

2.1 ZLD process layout

Figure 2 depicts the entire ZLD system including the membrane brine concentrator. The FO and OARO MBC and the two-pass RO unit are numerically modelled to determine which technology is the superior brine volume minimisation solution. The pre-treatment and brine crystalliser steps are excluded from the comparison. The entire ZLD process comprises of (Pendergast et al. 2016):

Pre-treatment processes: The waste stream is expected to have a total dissolved solid (TDS) content ranging between 25 g/L and 45 g/L. Due to this variability of the wastewater quality and the high concentration factor of the ZLD system, several pre-treatment processes are required to ensure an uninterrupted operation of the ZLD system. Scaling in the ZLD system is prevented by firstly softening the wastewater stream using chemical precipitation. This treatment step is followed by a multimedia filtration step and a weak acid cation exchange softening process.

Two-pass RO unit: The two-pass RO unit has two purposes, namely to pre-concentrate the softened feed stream for the MBC system and to polish the permeate to the product water (i.e. boiler make-up water) specification of $TDS < 100\,mg/L$. Concentrating the MBC feed stream reduces its size and takes advantage of the low energy demand of RO in the lower TDS range.

Membrane brine concentrator: The concentrate from the first RO pass is directed to the counter-flow FO (or OARO) membrane module. The high-pressure pumps and energy recovery devices (ERD) that are indicated in figure 2 are only utilised when the MBC is operated in the OARO configuration. However, both the FO and OARO MBC achieve the desired brine concentration using three stages and employing a thermo-responsive DS comprising of an ammonia and carbon dioxide mixture. The diluted draw solution (DDS) exiting the first stage S_1 of the membrane module is sent to the draw recovery distillation column (DC2) where the draw solutes are volatilised as NH_3 and CO_2 gas. The gases are condensed and mixed with a fraction of the DDS stream to give the CDS to be reused in the membrane process. The intermediate product water from DC2 is mixed with the softened feed stream and the concentrate from the secondary RO pass, This mixed stream is then directed to the RO system for polishing.

Reverse diffusion of the draw solutes into the FO/OARO feed stream will result in the loss of the draw solute if it is not recaptured. This is prevented by recovering the draw solutes in the concentrated brine stream using another distillation column, termed the brine stripper (DC1). The vapor stream from DC1 is sent to DC2 to be further concentrated while the heated brine stream exiting DC1 is pumped to the brine crystalliser at a TDS of $220\,g/L$. By utilising two distillation columns, the energy consumption of the MBC system increases, Although more than 99.75 % of the DS is retained in the system, which minimises its replenishment costs (Coday et al. 2014)).

In the FO MBC process, the concentrated draw solution (CDS) has a composition ranging between 4.0 M to 6.0 M on a carbon basis. The DS is thermally regenerated using plant steam (5 bar, saturated) as the energy source.

Brine crystalliser: The brine crystalliser is the most energy intensive process and removes the remaining liquid to crystallise the slurry. The distillate is recovered and mixed with the RO permeate and used as boiler make-up water.

2.2 Simulation set-up

As stated in the previous section, only the FO/OARO MBC and the two-pass RO system are numerically modelled. The design specifications and modelling assumptions are summarised in this section.

Firstly, it is assumed that the only solutes present in the system are $NaCl$ and the thermo-responsive draw solute due to the extensive pre-treatment. Thus, the fouling effect on the membrane and thermal process efficiency is not modelled. Additionally, the maximum draw solute concentration in the MBC system is limited to below its saturation point to prevent issues associated with precipitation.

Secondly, an iterative approach is chosen to determine the steady state operation of the modelled process. The membrane-based processes are simulated in Matlab using the same model that was previously developed and validated in Peters & Hankins (2019). Meanwhile, the DSR process with the two distillation columns is simulated with the help of ASPEN Plus. The function 'actxserver' is utilised in Matlab to communicate back and forth with ASPEN Plus. This direct link between Matlab and ASPEN Plus is original, as previously Excel had to be incorporated as an intermediate communicator, which significantly increased the simulation time (Claumann et al. 2015, Fontalvo

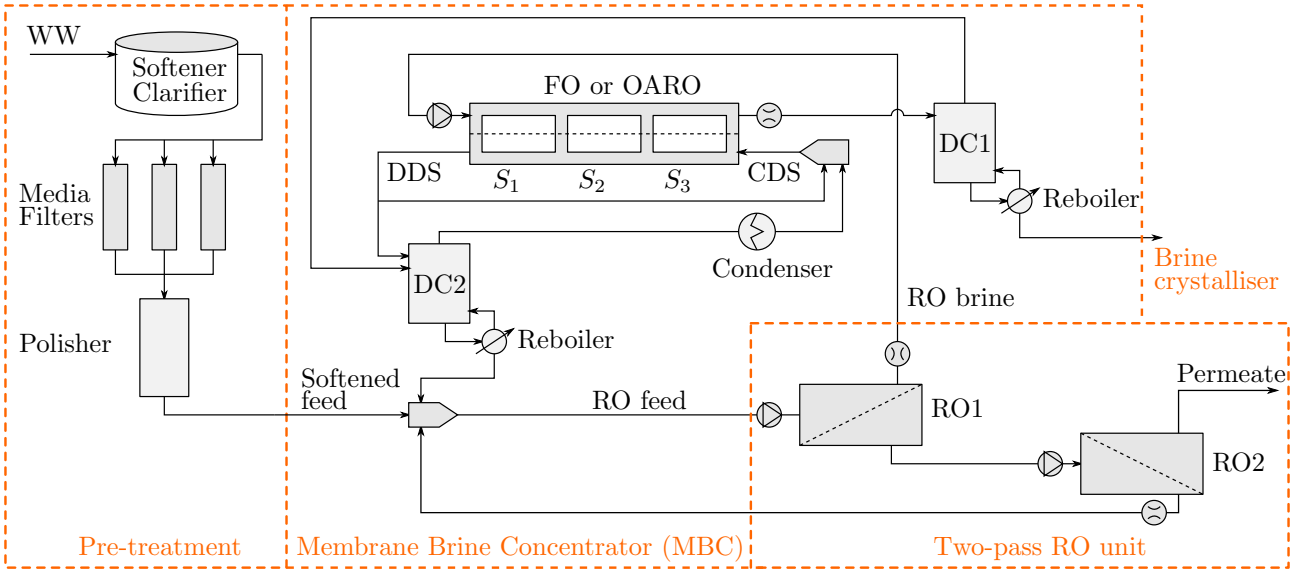

Figure 2: The FO zero-liquid discharge process installed at the Changxing coal-fired power plant, China. Adapted from Pendergast et al. (2016).

Alzate 2014). The algorithm is depicted in figure 3 and works as follows:

Step 0: Due to the intertwined process layout, the FO/OARO feed and draw stream, as well as the RO2 concentrate stream must be assumed in the first iteration, as they are unknown and are required to solve the steady state simulation.

Step 1: As starting point of each iteration, the 3-stage counter-current FO/OARO membrane model is solved. Each stage contains several pressure vessels in parallel so that the feed flowrate per vessel is given by Q_{MBC}. The numerical findings presented by Xiao et al. (2012) show that a counter-current flow arrangement has several advantages over a cocurrent flow arrangement, such as a more uniformly distributed water flux along the FO/OARO module. Therefore, in this work, all FO/OARO membrane modules are operated in a counter-current flow arrangement. The water flux and solute flux governing equations are solved explicitly on a finite set of iteration segments along the membrane module. The concentration of the draw solution and the mass flowrate at the module outlet are obtained with the shooting method (Xiao et al. 2012). More information regarding the FO/OARO membrane system is given in section 2.4.

Step 2: The newly determined DDS, CDS and FO/OARO brine stream information are communicated from Matlab to ASPEN Plus to solve the DSR system. The DSR set-up remains unchanged for all simulations and is described in more detail in section 2.5.

Step 3: With the MBC modelled using steps 1 and 2, the next step is to model the two-pass RO unit. The softened feed is firstly mixed with the RO2 concentrate and the intermediate product water from the MBC system. The two-pass RO unit is solved using the same solution procedure and governing equations as stated in Step 1. More information regarding the RO system is given in section 2.4.

Step 4: In each iteration, the only variable adjusted to achieve the desired brine concentration of 220 g/L (3.76 M) $NaCl$ is the CDS concentration. Thus, a new estimate of the required CDS concentration is interpolated using the concentration of the brine stream exiting DC1 and the current estimate of the CDS concentration. The new estimate of the required CDS concentration is then achieved by adjusting the recirculation rate of the DDS stream based on the concentration and volume of the condensed vapour stream from DC2.

Step 5: Steady state operation is reached once all flow streams converge and the overall mass conservation error is below 0.1 % of the inlet salt and water flowrate. Additionally, it is tested whether the desired brine concentration is reached using the given input parameters and the new interpolated CDS concentration. The iterative process is repeated at Step 1 until convergence is achieved.

2.3 The draw solution

While theoretically any draw solution can be employed in FO and OARO operation, the $NH_3 - CO_2$ thermo-responsive DS is chosen and evaluated here according

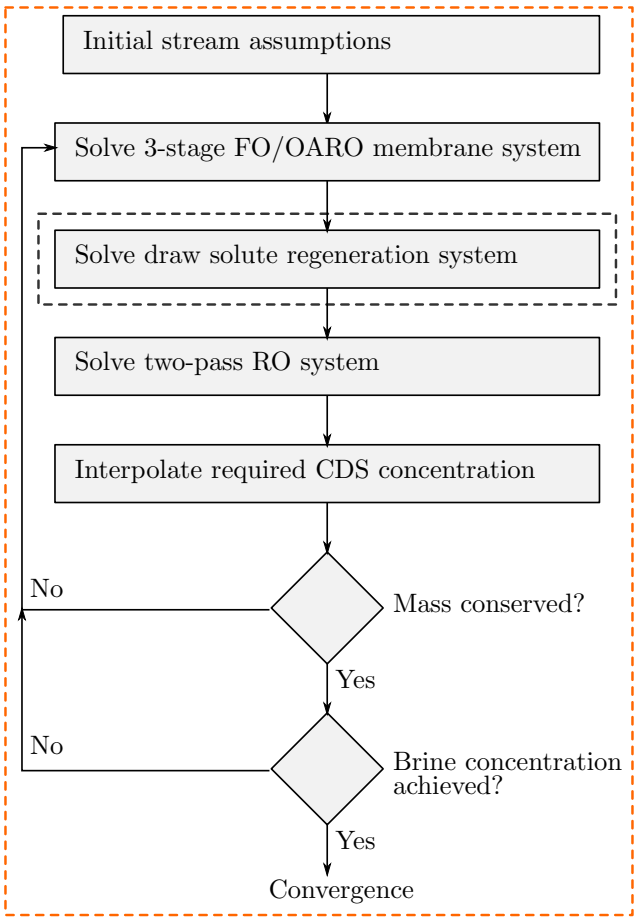

Figure 3: The simulation algorithm of the FO/OARO MBC and the two-pass RO system. The orange box indicates the commands run in Matlab whereas the gray box indicates the command run in ASPEN Plus. Communication and sharing of stream data between the two programs is initiated using the 'actxserver' function in Matlab.

to the following characteristics of an ideal draw solution (Luo et al. 2014):

High solubility and low molecular weight: These properties allow the draw solute to produce a high osmotic pressure. As shown in figure 4, the achievable osmotic pressure π of the $NH_3 - CO_2$ thermo-responsive draw solution mainly depends on the ammonia to carbon dioxide ratio (N/C) and the draw solute concentration (displayed on a carbon basis). As indicated in the figure, higher N/C ratios result in a stronger draw solution. A highly concentrated DS with a high N/C ratio is required to overcome the osmotic pressure of the final brine stream (indicated by the horizontal red line). It is important to note that the figure indicates the osmotic pressure of the bulk streams. Actually a significantly higher concentrated DS is required due to internal and external concentration polarisation (explained in section 2.4). Therefore, a high N/C ratio of 2.4 is chosen for the numerical simulations. This N/C ratio was also chosen by Zeng et al. (2017).

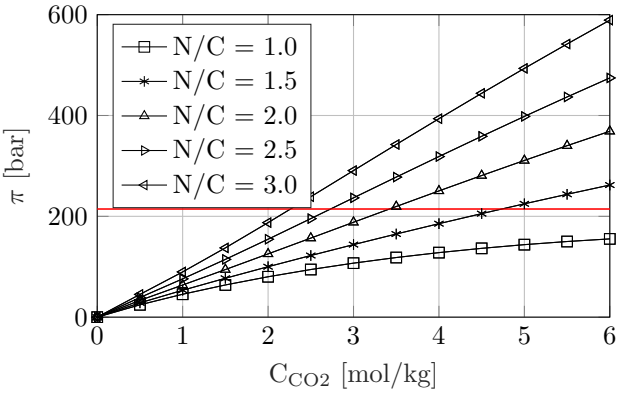

Figure 4: The osmotic pressure of the $NH_3 - CO_2$ thermo-responsive DS for various ammonia and carbon dioxide ratios (N/C) and draw solute concentrations on a carbon basis. The horizontal red line indicates the osmotic pressure of the final $NaCl$ brine stream with a concentration of 220 g/L. The osmotic pressures are determined using ASPEN Plus with the DSR set-up given in section 2.5.

Low viscosity: A lower viscosity of the DS reduces the internal concentration polarisation, which seriously hinders the water flux, and its pumping costs. ICP occurs in the porous support layer of the asymmetric TFC membrane and is more severe for viscous substances. ICP cannot be eliminated by enhancing turbulence or increasing the cross-flow velocity (Wang et al. 2010). In terms of the $NH_3 - CO_2$ draw solution, no issues regarding its viscosity have been mentioned in pilot and industrial scale testing (Pendergast et al. 2016, McGinnis et al. 2013). Furthermore, the $NH_3 - CO_2$ draw solutes are fast diffusing, which is further ideal to minimise ICP (McGinnis et al. 2013).

Low reverse solute flux: Due to the composition of the draw solution, ammonia and carbon dioxide do not fully disassociate and thus their uncharged species are not effectively rejected by the membrane causing a high reverse solute flux. As stated in McGinnis et al. (2013) and Hancock & Cath (2009), the reverse solute flux of the $NH_3 - CO_2$ thermo-responsive draw solutes is nearly an order of magnitude higher through asymmetric CTA membranes and three times higher through TFC-FO membranes in comparison to sodium chloride. This high reverse solute flux is problematic and is thus counteracted by including a secondary brine stripper (DC1) in the MBC system to maximise draw solute regeneration.

Ease of regeneration: The draw solute should be easily separable from freshwater in the regeneration step. Increasing the draw concentration inevitably increases the required energy of desalination. However, the vapour pressure of the thermo-responsive DS considerably exceeds that of water, which is desirable as the draw solute can be

easily vaporised in a distillation process operating at relatively low temperatures (McCutcheon et al. 2005). Although the draw solute decomposes at low temperatures (60 °C at 1 atm (McGinnis & Elimelech 2007)), the distillation column still has to be operated at significantly higher temperatures to completely remove any ammonia trace ($< 1\,ppm$) from the brine and product stream (Zhou et al. 2015).

Reusable: The draw solute should not lose its ability to generate its initial osmotic pressure after its regeneration. Otherwise it must be purged and replaced at an additional cost. Liquid-gas separation requires complex distillation and recondensation equipment to regenerate the draw solute (Dong et al. 2016). The thermolytic salt is not thermally stable (i.e. volatile) and thus complicating the gas containment in the system (Shon et al. 2015).

Non-toxic: Toxic solutes in the brine stream or in the final freshwater product can have detrimental effects. Ammonia is toxic above a certain threshold, hence the final water quality needs to present less than 1 ppm of ammonia (including related species such as ammonium and carbamate) in the permeate and brine stream to adhere to the limits specified in the Guidelines for Drinking Water Quality (WHO) (Zhou et al. 2015, Chekli et al. 2016).

2.4 The membrane processes

A, B and S values of the utilised RO and FO/OARO membranes are given in table 1.

Table 1: Membrane properties of the simulated RO and FO/OARO membranes.

Name	A [LMH/bar]	B [LMH]	S [mm]
SW30-HRLE [a]	1.13	0.08 (NaCl) 0.12 (DS) [b]	12.5
HTI-TFC [c]	3.16	0.55 (NaCl) 1.21 (DS) [d]	0.553

[a] (DOW Water Solutions 2017)
[b] Assumed from (Zhou et al. 2015)
[c] (Boo et al. 2015)
[d] (Zhou et al. 2015)

In the two-pass RO system, RO1 and RO2 are operated at 80 bar and 40 bar, respectively. Furthermore, the feed flowrate for each RO pressure vessel is kept constant at 12 m^3/h (Peters & Hankins 2019). Each RO pressure vessel is chosen to have a common number of 7 membrane modules with each having a membrane area of 37 m^2 (DOW Water Solutions 2017).

As shown in Chen & Yip (2018) and Peters & Hankins (2019), OARO can achieve the same recovery as MSRO and HPRO, but at operating pressures below the membrane burst pressure, ensuring it is technically feasible. In addition, OARO offers a better permeate quality than the MSRO process. Low operating pressures in OARO are possible, as a draw solution is utilised to lower the osmotic pressure difference ($\pi_D < \pi_F$) across the membrane (Kim et al. 2018). This combination of both FO and RO working principles allow for the dewatering of highly saline streams. For example, a theoretical study performed by Bouma & Lienhard (2018) found that the split-feed counterflow reverse osmosis (i.e. OARO) process could concentrate a brine stream up to 200 g/kg, while the process is operated at a maximum pressure of 68 bar.

In the MBC system, the FO/OARO membrane section consists of 3 stages (Pendergast et al. 2016) with each pressure vessel containing 7 membrane modules. The active membrane area of each FO and OARO membrane module is equivalent and estimated at 15 m^2 (Kim et al. 2017). As mentioned in section 2.2, the feed flowrate per pressure vessel Q_{MBC}, the operating pressure P_{MBC} and the flowrate ratio RR are varied to determine the optimal FO and OARO MBC operation. Kim & Park (2011) tested a single 4040 spiral-wound FO membrane module with a maximum feed flowrate of 1.08 m^3/h. Thus, the upper limit of Q_{MBC} for each pressure vessel containing 7 membrane modules is set at 7 m^3/h.

The tested P_{MBC} range is limited to 1 bar to 48.3 bar, as a minimum transmembrane pressure of 1 bar is required in FO to overcome the feed channel pressure losses (Kim & Park 2011). According to Straub et al. (2014), the maximum achievable membrane burst pressure for a commercially available thin-film composite (TFC) FO membrane is 48.3 bar, which is chosen here as upper limit of the membrane burst pressure of FO membranes. The RR range is chosen more arbitrarily and is varied between 0.3 and 0.7. As argued in Peters & Hankins (2019), the RR value is below 1 in practice, as the draw spacer in the membrane module must be more dense than the feed spacer to prevent membrane deformation under hydraulic feed pressures.

2.5 The draw solute regeneration (DSR) system

Both the FO and OARO MBC are operated with the equivalent heat integrated DSR system, which is depicted in figure 5. Thus, the ASPEN set-up described here remains unchanged and applies for all the FO and OARO MBC simulations.

As mentioned in section 2.3, two distillation columns are required to completely recover the volatile draw solutes so that less than 1 ppm of ammonia (including related species such as ammonium and carbamate) remains in the intermediate product and brine stream. The set-up of the distillation columns in ASPEN Plus is similar to that presented by Zhou et al. (2015). An instantaneous chemical equilibrium-stage model is used with the ENRTL-RK thermodynamic method to simulate the following complex reversible reactions occur-

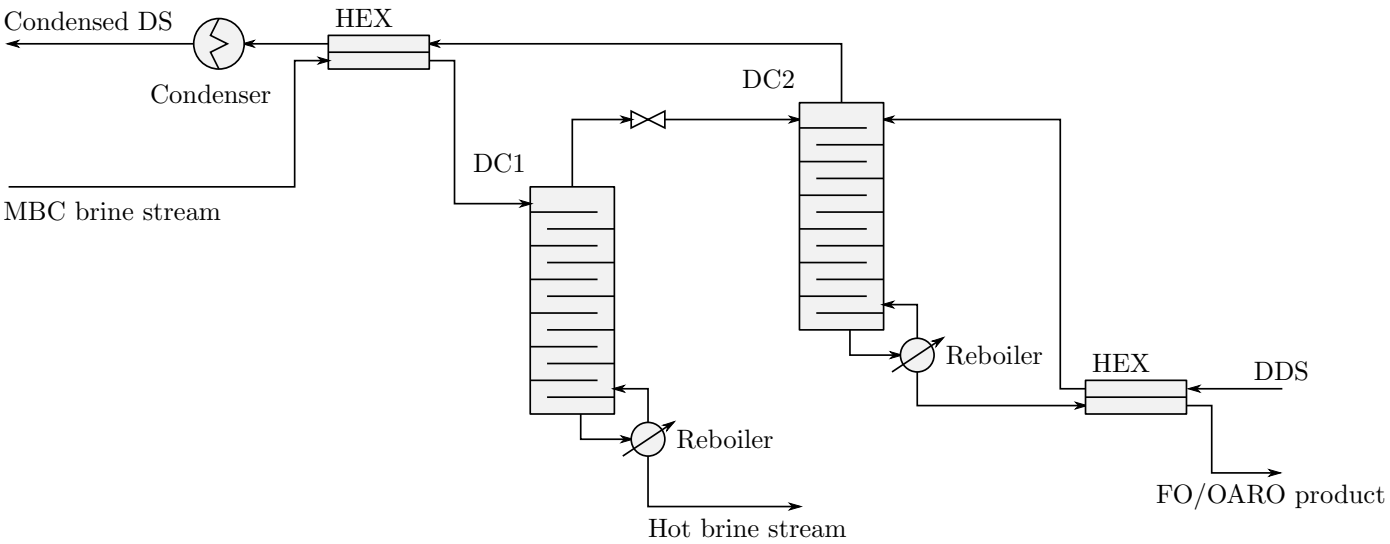

Figure 5: The draw solute regeneration system with heat integration. Adapted from Pendergast et al. (2016).

ring in the distillation process (Jilvero et al. 2014):

$$2\,H_2O \leftrightarrow H_3O^+ + OH^- \quad (1)$$

$$CO_2 + OH^- \leftrightarrow HCO_3^- \quad (2)$$

$$HCO_3^- + H_2O \leftrightarrow CO_3^{2-} + H_3O^+ \quad (3)$$

$$NH_3 + H_2O \leftrightarrow NH_4^+ + OH^- \quad (4)$$

$$NH_3 + CO_2 + H_2O \leftrightarrow NH_2COO^- + H_3O^+ \quad (5)$$

$$NH_4HCO_3\,(s) \leftrightarrow NH_4^+ + HCO_3^- \quad (6)$$

The last equation is not included in the simulation, as the maximum concentration of the draw solution is kept below its solubility limit. Furthermore, equation (2) and equation (5) are the rate-determining reactions, but are here assumed to be instantaneous and thus at equilibrium. As shown by Zhou et al. (2015), model inaccuracies arising from neglecting reaction kinetics occur chiefly at sub-atmospheric pressures. Sub-atmospheric operating pressures are, however, not considered, as an additional compressor will be required under such conditions to achieve complete condensation of the draw solution. This increases the capital cost and the electrical energy consumption.

Pendergast et al. (2016) considers that the distillation columns are operated at atmospheric pressure (i.e. 1 bar) and driven by 5 bar saturated steam. However, running the distillation columns at pressures closer to the saturation vapour pressure of the draw solution allows for the use of lower temperature heat sources. Therefore, the possibility exists to integrate low-grade waste heat (LGWH) as an energy source for the DSR system, which is discussed in greater detail in section 3.3.2.

As shown in Petchers (2012), typical steam condensing temperatures range from 40 C to 60 C, depending on the type of condenser utilised. Here, it is assumed that a water-cooled condenser can achieve a constant condensation temperature of 40 C. It is further assumed that the DC1 and DC2 column pressure vary according to the associated condenser pressure. Due to pressure losses in the system, DC1 and DC2 operate at column pressures that are 0.05 bar and 0.025 bar above the achievable condenser pressures, respectively.

The minimum approach temperature and the heat transfer coefficient in both HEX units is set to 2.5 C and 850 W/m^2 K, respectively (Cengel & Ghajar 2014). The same heat transfer coefficient is used for the condenser, whereas the reboiler heat transfer coefficient is set at 570 W/m^2 K. This is due to the fact that reboilers tend to foul faster because of the higher operating temperature and because non-volatile pollutants with higher fouling potential in the feed drop to the bottom of the column (Luyben 2013). Note that heat is not extracted from the hot brine stream exiting DC1, as operational issues can arise from cooling a highly concentrated waste stream. Also, energy is saved in the brine crystalliser if the feed remains warm (Pendergast et al. 2016).

2.6 Equivalent work principle

As the reboilers in the DSR system are thermally powered, the principal of equivalent work W_{Eq} is used to estimate the overall electrical energy consumption of the MBC and the two-pass RO system. The steam used to supply the required thermal energy to the reboilers of the DSR system is extracted from a steam turbine and is thus no longer available for electricity generation. Using the W_{Eq} method, thermal energy is assigned an electrical energy value, based on the capacity of that thermal energy to generate electricity in a steam turbine, which allows for a theoretical comparison of thermal process efficiencies. The equivalent work W_{Eq} (kWh/m^3) of the desalination process is calculated as follows (McGinnis & Elimelech 2007):

$$W_{Eq} = \frac{(h_{g,Steam} - h_{g,Cond})\,\eta_{Tur}}{3.6 \times GOR} + \sum SEEC \quad (7)$$

where $h_{g,Steam}$ and $h_{g,Cond}$ are the enthalpy (kJ/kg) of the extracted steam and the steam at the point where

it would normally enter the turbine condenser, respectively. As previously mentioned, the condenser temperature is assumed to be 40 C and is equivalent to the condenser temperature T_{Cond} of the DSR system. The turbine efficiency η_{Tur} is assumed to be 85 %, which is a typical value for the isentropic efficiency of a steam turbine (Cengel & Boles 2011). The gained output ratio (GOR) is calculated as follows:

$$GOR = \frac{h_{fg,Steam}}{\sum STEC} \tag{8}$$

where $h_{fg,Steam}$ is the vaporisation enthalpy (kJ/kg) of the utilised steam (which is saturated at 5 bar). The total specific thermal energy consumption (STEC) of DC1 and DC2 is given in kJ/kg. Furthermore, the specific electrical energy consumption (SEEC) of all the electrically driven equipment in the MBC and two-pass RO system is given in kWh/m^3.

2.7 Unit water cost calculation

The unit water cost is calculated as follows:

$$UWC = \frac{TAC\,[\$/year]}{Annual\,water\,production\,[m^3/year]} \tag{9}$$

where the total annual cost (TAC) is given by:

$$TAC = CF \times CapEx + OpEx \tag{10}$$

The capitalisation factor (CF) is assumed to be 10 %, as used in Bartholomew et al. (2018) for small-scale applications. The capital expenditures for the membrane systems are calculated by:

$$CapEx_{Mem} = F_{Mem} \sum (C_{Mem} + C_{HPP} + C_{BP} + C_{ERD} + C_{DS} + C_{PV}) \tag{11}$$

and the capital expenditure for the DSR system is given by:

$$CapEx_{DSR} = F_{DSR} \sum (C_{DC} + C_{HEX} + C_{Cond} + C_{Reb}) \tag{12}$$

The operational membrane and DSR expenditure are given by:

$$OpEx_{Mem} = \sum (O_{Elec} + O_{DS} + O_{Mem} + O_{ML} + O_{Chem}) \tag{13}$$

and:

$$OpEx_{DSR} = \sum (O_{Elec} + O_{CW} + O_{ML}) \tag{14}$$

Each factor in equation (11) to equation (14) is defined and given in table 2.

3 Results and discussion

3.1 Analysis of the DSR distillation columns

In this section, a parametric analysis of a single distillation column with heat integration is performed.

Figure 6a and figure 6b depict the reboiler temperature and heat duty per kilogram of feed. The draw solute concentration and the N/C ratio of the column feed solution are kept constant at 1 mol/kg on a carbon basis and 2.4, respectively. The achieved temperature profile in figure 6a at 0 mol/kg $NaCl$ is equivalent to that obtained in Zhou et al. (2015), which validates the set-up of the ASPEN simulation.

Solute diffusion across the FO/OARO membranes results in the cross contamination of the membrane draw and feed streams. Thus, traces of the DS are present in the brine stream and $NaCl$ in the diluted draw solution. Higher $NaCl$ concentrations in the column feed stream reduce the chemical potential of the volatile draw solutes. Hence, the temperature and the energy input of the reboiler must be raised to achieve the same target water purity of 1 ppm NH_3, as shown in figure 6a and figure 6b. Therefore, at high $NaCl$ concentration in the brine stream implies that operation of the brine stripper (DC1) is more energy intensive than that of DC2 per kilogram of feed.

Lower column pressures result in a lower reboiler temperature, which is beneficial for the utilisation of cheaper heat sources in the draw solute regeneration step. However, the minimum achievable column pressure without vapour compression is limited by the saturation pressure of the concentrated draw solution. As shown in figure 6b, the reboiler duty also reduces with the column pressure when $NaCl$ is present in the feed solution. This is owing to the fact that less water needs to be evaporated at lower column pressures to achieve the same residual ammonia concentration in the product.

Figure 6c and figure 6d depict the effect of the draw solute and $NaCl$ concentration on the reboiler temperature and its heat duty per kilogram of feed at a constant column pressure of 1 bar. Figure 6c shows that the reboiler temperature is relatively independent of the draw solute concentration at a constant column pressure. Thus, operation at a constant column pressure is not advised; it is suggested instead to operate at a constant condenser temperature. At lower draw solute concentrations, less ammonia and carbon dioxide are present in the vapour stream, which significantly reduces the saturation pressure of the vapour stream. Therefore, the column pressure and hence the reboiler temperature can be minimised at a constant condenser temperature.

The findings depicted in figure 6d indicate that the reboiler duty is less affected by the draw solute concentration at higher $NaCl$ concentrations. This means that the energy cost of DC1, which has a highly concentrated $NaCl$ feed, is not significantly reduced if lower reverse draw solute fluxes are achieved in the FO/OARO membrane section. However, the energy consumption of DC2, which is fed by the low salinity DDS stream, is more affected by lower draw solute concentrations.

Reasonable conclusions on the operation of DC1 and DC2 can be drawn from this analysis, as the interdependence of DC1 and DC2 is minimal. The operational

Table 2: Financial parameters for the calculation of the unit water cost

Capital financial parameters		Value
Practical investment factor	$F_{FO,OA}$ [a]	1.6
(Lang factor)	F_{RO} [a]	1.4
	F_{DSR} [b]	3.68
Membrane unit cost [a]	$C_{Mem,FO/OA}$	$50\,\$/m^2$
	$C_{Mem,RO}$	$30\,\$/m^2$
High-pressure and booster	C_{HPP}	$53\,\$/(m^3/h\,bar)$
pump costs [a]	C_{BP}	$53\,\$/(m^3/h\,bar)$
Energy recovery device cost [a]	C_{ERD}	$3134.7\,(Q_{ERD}\,[m^3/h])^{0.58}\,\$$
(Only employed if $P_F > 10\,bar$)		
Draw solute purchasing cost [c]	C_{DS}	$8.75\,\$/kg$
Pressure vessel unit cost [d]	C_{PV}	$1000\,\$/vessel$
Distillation column cost [e]	C_{DC}	$17640 * \varnothing^{1.066} * L^{0.802}\,\$$
Heat exchanger cost [e]	C_{HEX}	$7296\,(A_{HEX}\,[m^2])^{0.65}\,\$$
	C_{Cond}	$7296\,(A_{Cond}\,[m^2])^{0.65}\,\$$
	C_{Reb}	$7296\,(A_{Reb}\,[m^2])^{0.65}\,\$$
Operational financial parameters		**Value**
Electricity cost [a]	O_{Elec}	$0.075\,\$/kWh$
Draw solute replenishment cost [f]	O_{DS}	$0.01\,C_{DS}\,\$/year$
Membrane replacement cost [a]	O_{Mem}	$0.15\,C_{Mem}\,\$/year$
Maintenance and labour cost	$O_{ML,Mem}$ [a]	$0.02\,CapEx_{Mem}\,\$/year$
	$O_{ML,DSR}$ [b]	$0.04\,CapEx_{DSR}\,\$/year$
Chemical consumption cost [a]	O_{Chem}	$0.01\,CapEx_{Mem}\,\$/year$
Cooling water consumption cost [e]	O_{CW}	$0.016\,\$/kWh$

[a] (Bartholomew et al. 2018) [b] (Lara et al. 2012)
[c] (Johnson et al. 2018) [d] (Lu et al. 2007)
[e] (Luyben 2013)
[f] Assumed value to model the DS loss through the product and brine stream

conditions of DC2 are only slightly affected by those of DC1, because the vapour passed from DC1 to DC2 is less voluminous than the DDS stream entering DC2. For that reason, it is less pivotal.

3.2 Parametric optimisation of the FO and OARO integrated ZLD flow processes

In this section, a parametric analysis of the FO and OARO integrated ZLD processes is performed to ensure that the conclusions drawn apply to a wide range of operational conditions. Nevertheless, global optimality cannot be guaranteed by this model, as the process configurations, and thus the cost and performance data are subject to the unique case specifications and the process parameters that are established by this model. However, this comparison offers insights into whether OARO operation can in fact be more energy efficient than FO.

The base case parameters are set as $N/C = 2.4$, $Q_{MBC} = 5\,m^3/h$, $RR = 0.5$ and the inlet salinity $S_{In} = 45\,g/L$. Furthermore, the OARO process is operated at a transmembrane pressure of 48.3 bar, which corresponds to the maximum membrane burst pressure as stated in section 2.4. Comparatively, the FO process is only operated at a 1 bar transmembrane pressure.

Figure 7 depicts the equivalent electrical energy consumption for the two-pass RO unit (black), the DC1 (dark grey), the DC2 (light grey) and the three-stage FO/OARO membrane unit (orange), respectively, under various operational conditions. The results for the FO and OARO integrated ZLD processes are represented in the left-hand and right-hand columns, respectively.

Pendergast et al. (2016) state that the actual steam-driven MBC with a two-pass RO system consumes roughly 4 kWh of electrical energy per cubic meter of product water. The thermal and cooling demand is estimated to vary between 20 kWh/m^3 to 200 kWh/m^3. These estimates seem to agree well with the results obtained here for the base case, the FO integrated ZLD process. In the FO base case, the electrical, thermal and cooling demand are 4.54 kWh/m^3, 141.58 kWh/m^3 ($W_{Eq} = 9.94\,kWh/m^3$) and 114.58 kWh/m^3, respectively. Furthermore, the maximum concentration of the concentrated draw solution is 6.18 mol/kg, which is just above the range of draw solution concentrations (4 mol/kg to 6 mol/kg) mentioned in Pendergast et al. (2016).

The W_{Eq} of the FO and OARO base case are 14.5 kWh/m^3 and 12.93 kWh/m^3, respectively. Under these conditions, the total energy savings amount to 10.83 % when using the OARO integrated ZLD process. This is achieved due to a lower thermal energy demand (109.24 kWh/m^3), although the electrical energy demand is slightly higher (5.24 kWh/m^3) due to the high pressure operation of the OARO MBC. Ad-

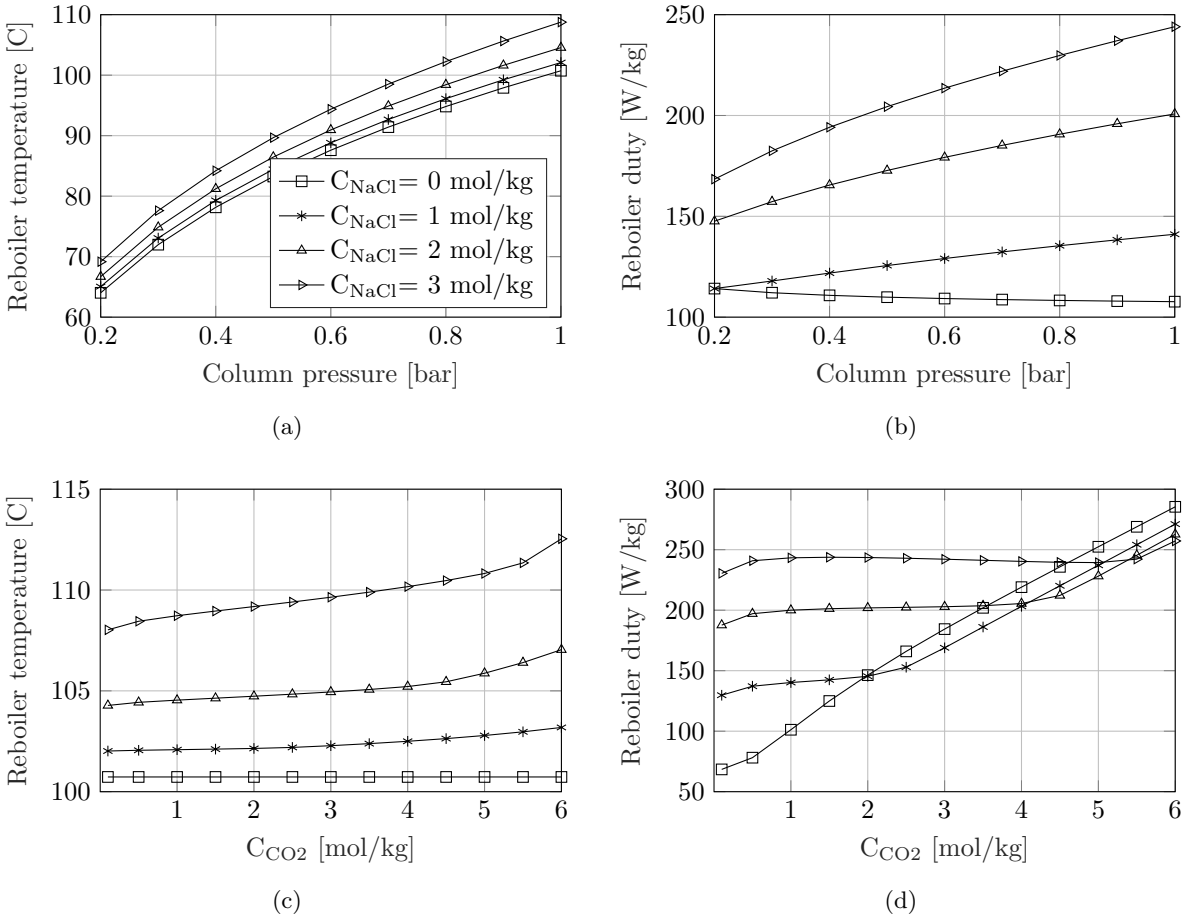

Figure 6: Parametric analysis of a single distillation column for various $NaCl$ feed concentrations. Figures (a) and (b) depict the effect of the column operating pressure on the reboiler temperature and its heat duty per kilogram of feed solution containing a 1 mol/kg thermo-responsive draw solution on a carbon basis and a N/C ratio of 2.4. Figures (c) and (d) depict the effect of the draw solute on the reboiler temperature and its heat duty per kilogram of feed at a constant column pressure of 1 bar. The N/C ratio of the feed solution is also kept constant at 2.4.

ditional savings are incurred by a lower cooling load (87.93 kWh/m^3), with the maximum concentration of the concentrated draw solution at only 3.75 mol/kg.

In the following subsections, a single operational parameter is altered while the remaining parameters are kept constant:

3.2.1 Effect of N/C ratio:

Increasing the N/C ratio of the thermo-responsive draw solution leads to an overall reduction in the energy consumption of the FO integrated ZLD process. The main energy savings are achieved in DC2, because the DDS feed stream is less voluminous and contains lower ammonia concentrations. This is due to the fact that higher N/C ratios enhance the osmotic potential of the draw solution at equivalent ammonia concentrations, as shown in figure 8. However, the energy consumption of DC1 increases with the N/C ratio, as additional energy is required to strip the more soluble, excess ammonia from the saline brine. Another drawback of larger N/C ratios is that the condenser pressure is raised, which leads to higher DC1 and DC2 reboiler temperatures. Darde et al. (2012) have shown that this occurs because the partial pressure of ammonia rises when $N/C > 2$, while the partial pressure of carbon dioxide remains relatively constant. Due to this existing trade-off between reboiler temperature and energy consumption, an intermediate N/C ratio of 2.4 is chosen.

The required CDS concentration in the OARO base case is approximately 39.3 % less than that for its FO counterpart. Because of that, the extent to which the draw solute concentration varies with changes of the N/C ratio is minute, resulting in an insignificant effect on the overall energy consumption of the OARO integrated ZLD process, as seen in the right-hand column.

3.2.2 Effect of the FO/OARO feed flowrate:

For all cases, the recovery of the FO/OARO MBC unit remains approximately constant, as the final target brine concentration is fixed and the RO brine concentration varies only slightly with operational changes. To achieve the same recovery at higher feed flowrates Q_{MBC} means that the water flux has to increase, as less FO/OARO pressure vessels are required in parallel (i.e. the total membrane area decreases) to process the same overall feed rate. To achieve a higher wa-

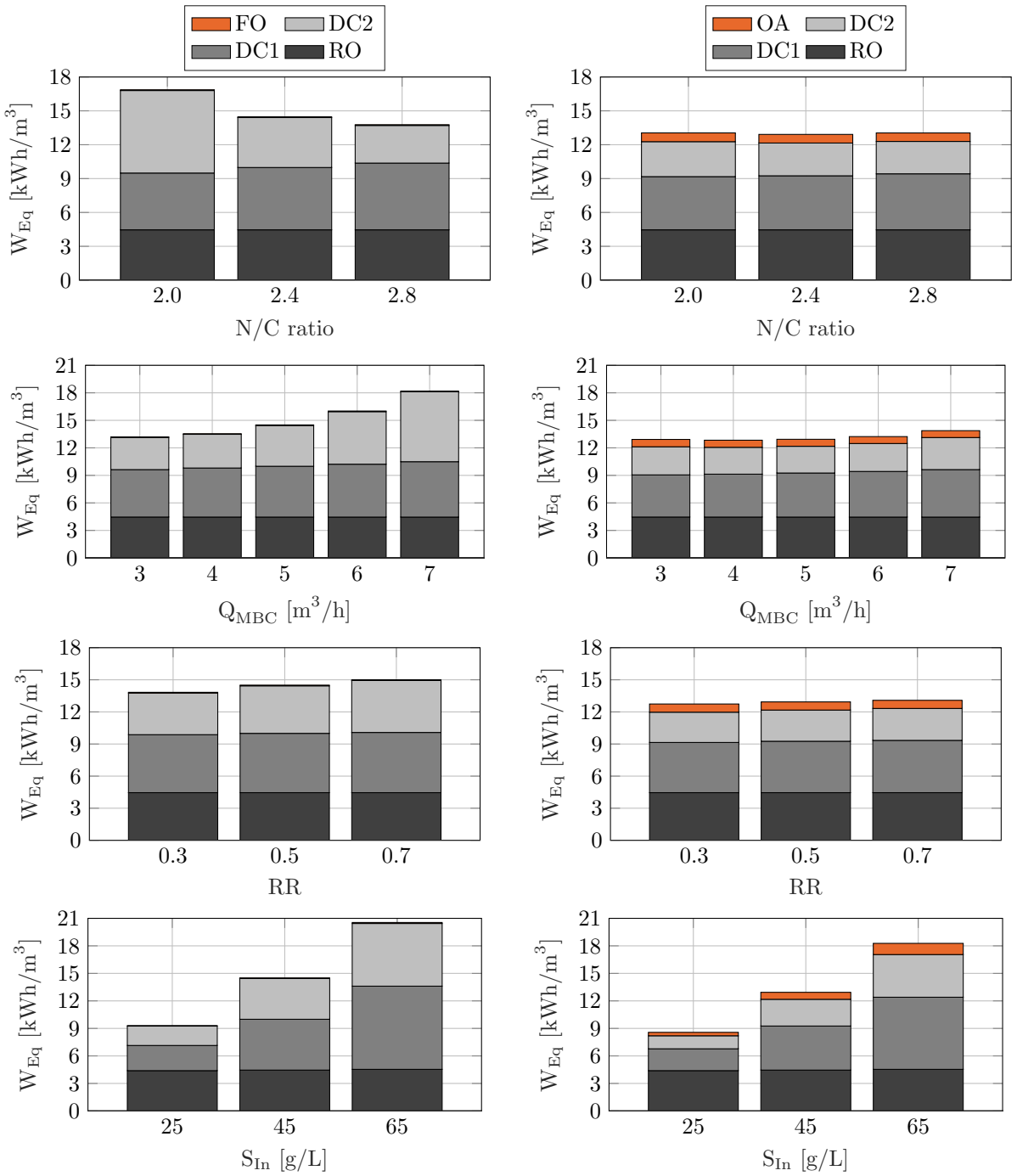

Figure 7: The equivalent work W_{Eq} of the FO (left column) and OARO (right column) integrated ZLD processes with respect to various operational parameters. The standard operational parameters are as follows: N/C is 2.4, Q_{MBC} is 5 m^3/h, RR is 0.5, T_{Cond} is 40 C, feed inlet salinity S_{In} is 45 g/L and 5 bar saturated steam is used as heat supply to the DSR system. The FO/OARO base case is always given by the central column in each figure.

ter flux, a stronger driving force is necessary and thus the draw solute concentration has to increase, as the hydraulic feed pressure of each technology remains unchanged. This increase in required draw solute concentration takes its toll on the overall process energy consumption. The increase in energy consumption is especially evident for DC2. However, high hydraulic pressure in the OARO process tends to limit the required increase in the draw solute concentration with the feed flowrate. Therefore, the energy consumption of the OARO integrated ZLD process is less affected by the change in feed flowrate, while the FO counterpart is significantly affected by it, as seen in the right columns of figure 7.

In terms of fouling, it is difficult to conclude whether a higher feed flowrate is preferred and whether membrane fouling is more likely in OARO or FO operation. Firstly, higher feed flowrates can impede or limit fouling of the membrane surface, as higher cross-flow velocities enhance the shear stress responsible for

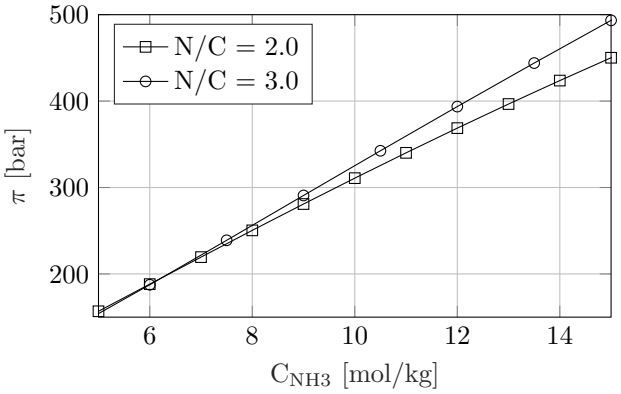

Figure 8: The osmotic pressure of the $NH_3 - CO_2$ thermo-responsive draw solution for two N/C ratios with respect to the ammonia concentration.

the detachment of foulants from the membrane surface (Franken 2009). Secondly, the water flux is another important indicator of the membrane fouling propensity. According to the critical flux theory, fouling is reversible if the membrane process is operated below the critical flux, but pronounced and irreversible once this flux is exceeded (Bacchin et al. 2006, Nguyen et al. 2019). The exact value of the critical flux is unknown for this process, as it depends on several factors including the membrane properties and the feedwater characteristics. Nevertheless, a lower water flux is still preferred to prevent irreversible fouling. Thus, according to the critical flux theory, a lower feed flowrate is beneficial because it leads to lower water fluxes. This conflicts with the previous statement that higher feed flowrates reduce the fouling rate via turbulence enhancement.

The average water flux in the first stage S_1 of the OARO base case is roughly 20.45 LMH and thus greater in comparison to the 17.34 LMH for the FO base case. On the other hand, the average water fluxes in the second (S_2) and third (S_3) stages of the OARO base case (10 LMH to 5.18 LMH) are slightly lower than that for the FO base case (10.44 LMH to 6 LMH). This suggests that irreversible biofouling, organic and/or colloidal fouling, which generally occur in the first membrane modules (Voutchkov 2018), are more likely for OARO than for FO operation. Nevertheless, irreversible scaling, which is more common in the final membrane modules (Voutchkov 2018), is more likely to occur for FO than for OARO operation due to the higher water fluxes in the last two membrane stages S_2 and S_3.

Figure 9 implies that the brine stream exiting the final stage S_3 of the OARO process is less contaminated by ammonia RSF than that of the FO process. As stated in Section 2.3, ammonia back diffusion can serve as nutrient source and thus promote increased biofouling on the feed side of the membrane. This suggests that OARO operation with the thermo-responsive draw solution may be less prone to biofouling than FO. Furthermore, the reverse solute flux of the thermo-responsive draw solution lessens with an increase of the feed flowrate, due to the higher water flux against which it must operate.

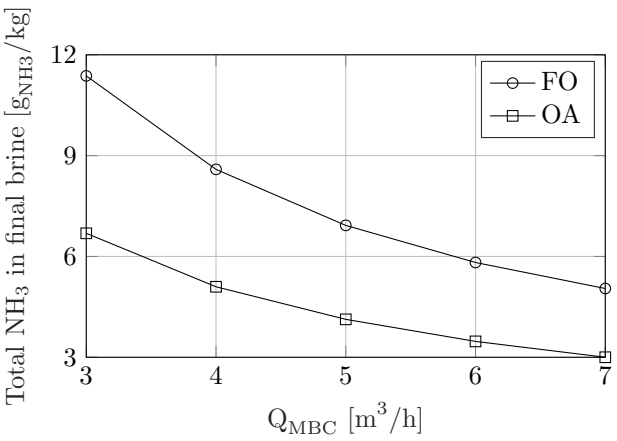

Figure 9: Total ammonia concentration in the brine stream exiting the final FO/OARO stage at various Q_{MBC}.

Several other studies indicate that FO has a lower fouling propensity than pressure-driven membrane processes, as the fouling layer remains loosely attached to the membrane instead of being compacted onto the membrane surface at high hydraulic pressures (Lotfi et al. 2017, Lee et al. 2017, Cai & Hu 2016). However, opposite to this common claim, the experimental findings presented by Siddiqui et al. (2018) show that FO is in fact more prone to alginate fouling than RO and that the hydraulic operating pressure was not found to play a critical role in foulant layer compaction. Furthermore, Tow et al. (2018) states that under the same hydrodynamic conditions, FO has a higher scaling resistance than RO, which is theorised to be due to the difference in the membrane material, but with organic foulants present, both RO and FO experienced a similar flux decline. All of these somewhat contradictory findings make it difficult to conclude which of the two technologies is less prone to fouling.

In terms of the energy consumption, it would be ideal to eliminate the costly brine stripper from the MBC process by minimising the reverse solute flux. This seems more achievable via OARO than FO operation at high Q_{MBC}, as shown in figure 9. At the maximum feed flowrate, the ammonia concentration in the MBC brine stream will be 40.5 % lower for the OARO integrated ZLD process. However, a brine stripper is still required, as 3 g/kg of ammonia is still notably higher than the target ammonia concentration of 0.001 g/kg.

The OARO integrated ZLD process at low Q_{MBC} values achieves the desired brine concentration using the lowest draw solute concentration. Operating with a more dilute draw solution also results in a lower saturation pressure of the vapour stream to be condensed. The lower saturation pressure directly translates into lower column operating pressures and hence lower reboiler temperatures. These trends are depicted in figure 10 and show that OARO is more suited for the integration of low grade heat sources. At an equiv-

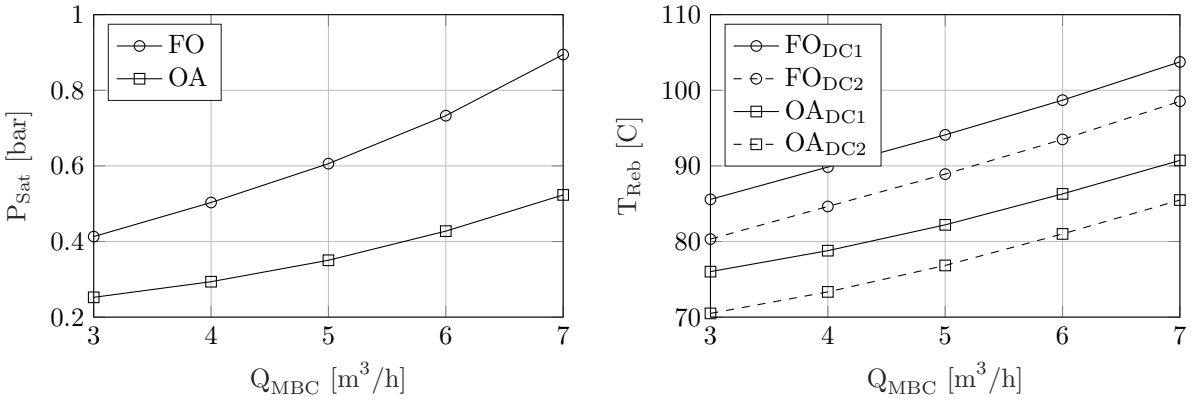

Figure 10: The saturation pressure and the DC1 and DC2 reboiler temperature for the FO and OARO DSR system at various Q_{MBC} and at a constant condenser temperature of 40 C.

alant feed flowrate, the reboilers in the DSR system of the OARO MBC can be operated at temperatures approximately 12 C lower than their FO counterparts.

3.2.3 Effect of RR:

RR is defined as the ratio between the draw and feed flowrate. At lower RR values, the FO/OARO draw stream is less voluminous but more concentrated. In total, the quantity of draw solution to be regenerated is slightly reduced with lower RR values. Hence, DC1 and DC2 consume less energy and can be operated at lower temperatures. However, the energy consumption (see figure 7) and reboiler temperature of both FO and OARO integrated ZLD processes are relatively insensitive to the RR ratio.

As reasoned in Peters & Hankins (2019), lower RR values are also more practical. The draw spacer in the OARO draw channel must be more dense than the feed spacer to prevent membrane deformation under high feed pressures. That being so, lower draw flowrates reduce the pressure loss in the more constrained draw channel.

3.2.4 Effect of the inlet salinity:

All figures in figure 7 indicate that the energy consumption of the two-pass RO component remains relatively constant, irrespective of any operational changes. This even holds true at higher inlet salinities, as the recovery of the RO system reduces at higher inlet salinities while the outlet brine concentration remains unchanged. This lower system recovery at higher S_{In} and the constant inlet flowrate of 100 m^3 result in higher stream flowrates and salinities in the rest of the ZLD system. Therefore, the total energy contribution of the MBC (DC1, DC2 and FO/OA) increases with S_{In}.

3.3 Techno-economic comparison of the OARO and FO integrated ZLD processes

In this section, a techno-economic comparison of the FO and OARO base cases is performed for a (1) steam and (2) flue gas (i.e. low grade waste heat) powered reboiler. The comparisons are only performed for the base cases, as the operational parameters are already set to achieve reasonably low reboiler temperatures while simultaneously reducing the energy consumption, the maximum draw solute concentration (to prevent precipitation) and the membrane fouling propensity. The unit water cost is used to determine the economic feasibility of each process.

3.3.1 UWC of the steam powered FO and OARO base cases

The unit water cost of the steam and flue gas powered FO and OARO base cases is depicted in figure 11. As shown in the figure, the operational expenses dominate and in total contribute approximately 70 % to 76 % towards the overall cost of the steam driven FO and OARO integrated ZLD processes. Thus, the UWC calculation is especially sensitive to fluctuations in the operational financial parameters, which are stated in table 2. The UWC is presented for three different electricity costs, as this is in addition to the cooling water cost, the most sensitive variable. If the electricity cost increases from 0.05 $ to 0.1 $, the UWC increases by 16.7 % and 17.7 % for the steam driven FO and OARO integrated ZLD processes, respectively.

For the steam driven processes, a cost saving of approximately 15.5 % can be achieved when operating the MBC in OARO mode instead of FO mode for an equivalent electricity cost. These savings are mainly conferred by reducing the energy consumption of the DSR system, as lower draw solute concentrations are required when operating in OARO mode. Although OARO requires high-pressure pumps and energy recovery devices, the additional cost incurred by this equipment is negligible in comparison to the overall operational and capital cost savings.

3.3.2 UWC of the LGWH powered FO and OARO base cases

The findings in section 3.2 and section 3.3.1 indicate that the DSR unit is the primary energy consumer, as

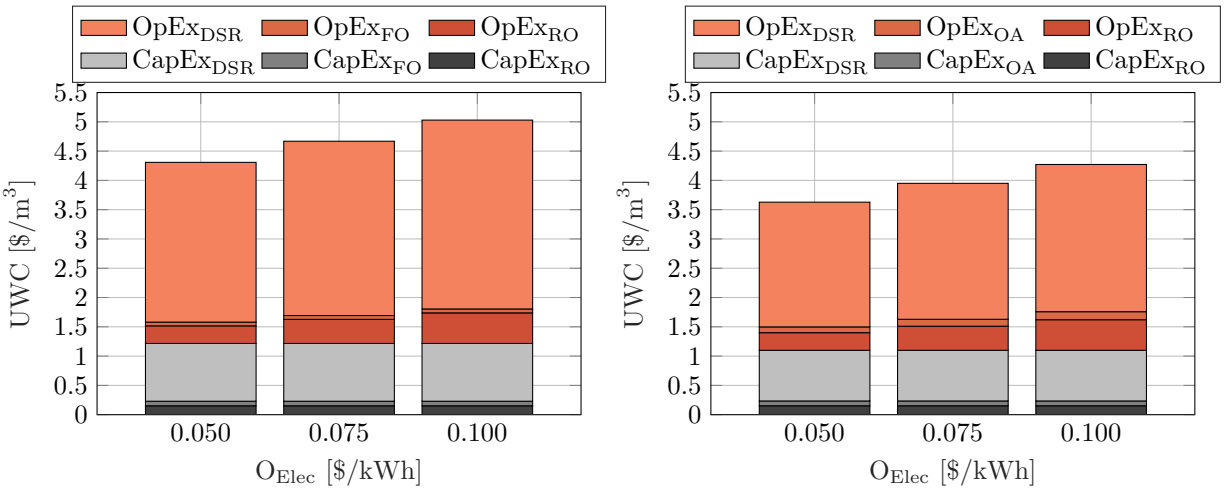

(a) Steam powered FO integrated ZLD process

(b) Steam powered OARO integrated ZLD process

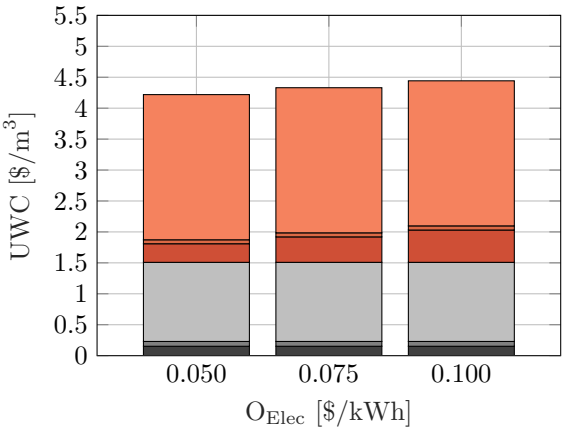

(c) LGWH powered FO integrated ZLD process

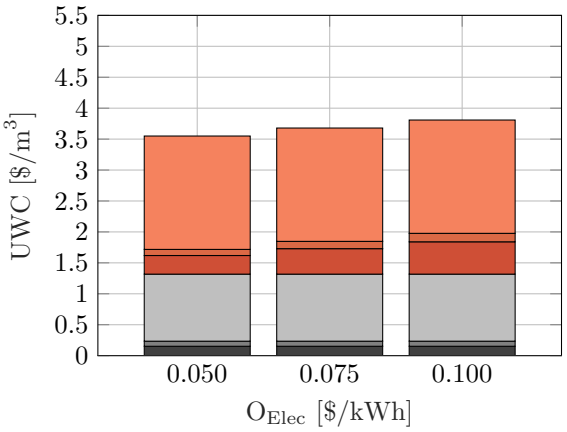

(d) LGWH powered OARO integrated ZLD process

Figure 11: Sensitivity analysis of the unit water cost for the FO and OARO base cases with respect to the electricity cost.

well as the most expensive process in the analysed ZLD system (excluding pre-treatment and brine crystallisation). Therefore, substituting the valuable steam heat source with a less costly one can significantly lower the overall cost of the ZLD system. A recent study by Gingerich & Mauter (2015) estimated that in the U.S. alone, more than 803 million GJ of heat at temperatures greater than 90 C were exhausted to the environment in 2012. Since the analysed ZLD system is located close to a coal-fired power plant, the available boiler hot flue gas comes to mind as a potential source of low-grade heat source. However, depending on the required reboiler temperature, other alternative low-grade heat sources, such as geothermal, nuclear or solar energy, can also be utilised in the desalination process.

The median flue gas temperature from coal-fired power plants was estimated by Gingerich & Mauter (2015) to be 128.4 C. This temperature is more than sufficient to drive the FO and OARO DSR system. As shown in figure 10, the minimum achievable DC1 and DC2 reboiler temperatures are 76 C and 70.6 C. These low reboiler temperatures are reachable by decreasing Q_{MBC} and operating the MBC in OARO mode rather than in FO mode. For example, the DC1 and DC2 reboiler temperature can be reduced by 12 C at any Q_{MBC} when choosing an OARO configuration of the MBC instead of an FO configuration. Thus, LGWH integration is more feasible via OARO than via FO operation of the MBC.

However, one issue arises when utilising flue gas as a heat source. While the heat transfer coefficient can reach up to 6000 W/m^2 K during the condensation of steam, a much lower heat transfer coefficient of 30 W/m^2 K to 300 W/m^2 K is achieved with flue gas because the gas density is lower and no phase change occurs (Cengel & Ghajar 2014). Furthermore, the relatively low temperature of the flue gas results in a reduced temperature difference in the reboiler. Both effects result in the requirement of a larger heat transfer area for the reboiler, which inevitably increases the capital cost of the DSR system.

The energy requirements of seawater RO desalination plants typically lie in the range of 4 kWh/m^3 to 8 kWh/m^3 while achieving a brine salinity of approximately 70 g/kg (Mezher et al. 2011). In the

present case, the final brine concentration reaches up to 190 g/kg while the electrical energy consumption can be reduced to 4.54 kWh/m^3 and 5.24 kWh/m^3 with LGWH integration for the FO and OARO base cases, respectively. This significant increase in system recovery for a similar energy consumption is a major advantage of LGWH integration. However, LGWH integration can only reduce the operational expenses of the DSR system to a certain level, as the cost associated with cooling water consumption and maintenance remain unchanged. As shown in figure 11c and figure 11d, LGWH integration is not very worthwile on economical and technical grounds if the electricity cost is low (0.05 $/kWh), as the UWC is only slightly reduced when compared to a steam powered system and the system layout and operation becomes more complex. On the other hand, at high electricity costs (0.10 $/kWh), the overall cost savings for both FO and OARO integrated ZLD processes with LGWH integration is approximately 11 %.

As stated in Voutchkov (2018), the industry average freshwater production cost is 1.1 $/m^3 for medium to large scale seawater RO desalination systems. With LGWH integration and OARO operation, the UWC of the MBC and the two-pass RO unit alone is still three to four times higher although the achievable electricity consumption falls in the range of a typical RO desalination plant. Another possibility to reduce the freshwater production cost is by increasing the scale of the operation. Increasing the scale of the plant reduces capital expenditures to an extent, as the design, development and construction costs are not directly linked to the plant's freshwater production rate. However, in this case the influence of the capital cost on the UWC is insignificant and thus the cost savings associated with increasing the plant scale are limited.

3.4 Comparing the FO and OARO MBC with the LSRRO and the standard OARO processes

As the parametric and the techno-economic study have proven, utilising an additional hydraulic driving force (OARO) can significantly reduce the cost, energy consumption and the DSR temperature of the purely osmotically driven membrane process (FO). However, it is still unclear whether combining OARO with a thermo-responsive DS offers any benefits in comparison to other novel membrane-based BVM techniques. To answer this question, the FO and OARO MBC are compared to the LSRRO system, which was proposed by Wang et al. (2020), and the standard OARO process with a non-responsive DS (i.e. NaCl), which is given by Bouma & Lienhard (2018). Both the LSRRO and the OARO process with the non-responsive DS are depicted in figure 12.

The simulation results from all three studies are presented in table 3. To allow for a fair comparison of the membrane-based ZLD processes, a single-pass RO system is utilised in the FO and OARO MBC instead of a two-pass RO system. Furthermore, for this comparison all processes are expected to concentrate a saline feed of 0.6M to 4M. This test case slightly differs from that in the previous sections, in which a saline feed is concentrated from 0.77M (45 g/L) to 3.76M (220 g/L). For this new test case, the equivalent work of the FO and OARO MBC are 11.1 kWh/m^3 and 9.3 kWh/m^3 when using a single-pass RO system and 5 bar saturated steam to power the DC reboilers.

There are two methods to further reduce the overall energy consumption of the FO and OARO MBC system. Firstly, heat pumps (i.e. vapor compression) can be utilised instead of steam to power the reboilers (Pendergast et al. 2016), or secondly, LGWH can be utilised to supply the required thermal load. Assuming that LGWH integration is possible, the FO and OARO MBC energy cost can be substantially reduced to 2.94 kWh/m^3 and 3.47 kWh/m^3, respectively.

In comparison, the calculated energy consumption of the 4-stage LSRRO is 5.14 kWh/m^3 when it is required to concentrate the same saline feed to 4M (Wang et al. 2020). However, in contrast to our simulation, the calculation of the specific electrical energy consumption performed by Wang et al. (2020) neglects 1) external concentration polarisation effects, 2) the pressure drop across membrane modules and 3) assumes that even the highly concentrated solution behaves ideally and conforms to the van't Hoff approximation. All of these simplifications can substantially increase the numerical error in the value of the simulated water flux, as shown by Bartholomew & Mauter (2019), and the actual SEEC of the LSRRO process (with a finite membrane area) is expected to be far higher than 5.14 kWh/m^3. Even under ideal LSRRO conditions, the OARO MBC with LGWH integration can outperform the LSRRO process and operate at a 32.5 % lower SEEC.

On the other hand, the calculation performed by Bouma & Lienhard (2018) for the standard OARO system with a non-responsive DS includes external and internal concentration polarisation. Their calculation shows that the conventional OARO process only requires 3.9 kWh/m^3 and is the most energy efficient technology to achieve the desired brine concentration. However, one main issue with this OARO process is that the achievable water fluxes in the final three membrane stages are very low ($< 1\,LMH$). Therefore, a total of 6 stages with large membrane areas are required to achieve the desired brine concentration. Furthermore, the OARO stages have to be operated at a maximum transmembrane pressure ΔP_{Max} of 68 bar, while the membrane's S-value is assumed to be only 564 μm, which is comparable to the membrane's S-value used in this study. These high operating pressures may inevitably lead to the failure of these thin OARO membranes. In contrast, the OARO MBC can be operated at lower hydraulic pressures and at economically feasible water fluxes ($> 5\,LMH$) when using a strong thermo-responsive DS.

As shown in figure 13, the OARO process can achieve brine concentrations of up to 245 g/kg when operated

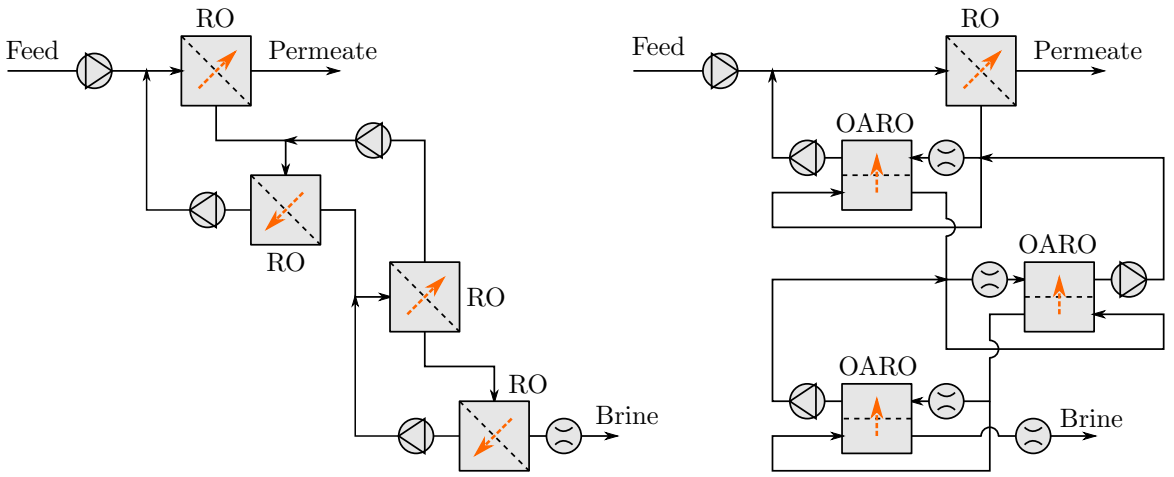

Figure 12: Schematics of a 4-stage low-salt-rejection RO (Wang et al. 2020) (left) and OARO process with a non-responsive draw solution (Bouma & Lienhard 2018) (right). The direction of the water flux is indicated by the orange arrows.

at technically feasible pressures (48.3 bar (Straub et al. 2014)) and draw solute concentrations ($\approx 6\,mol/kg$ on a carbon basis (Pendergast et al. 2016)). Theoretically, even higher recoveries can be achieved by the OARO system, as the required thermo-responsive DS concentration in the CDS stream CDS_{Th} could be increased beyond 6 mol/kg (on a carbon basis); the solubility limit of the thermolytic draw solution is approximately 13 M (Zhou et al. 2015). In any case, such high brine concentrations cannot be achieved by conventional OARO systems utilising non-responsive DS. Similarly, the FO MBC also cannot achieve such high brine concentrations without exceeding the suggested upper limit of CDS_{Th}.

The OARO MBC can achieve brine concentrations of up to 245 g/kg while operating at $W_{Eq} = 10.8\,kWh/m^3$ and a maximum reboiler temperature of 94.1C, whereas the FO MBC requires $W_{Eq} = 11.1\,kWh/m^3$ and a maximum reboiler temperature of 97.2C to achieve a lower brine concentration of 205 g/kg. This means that combining OARO with a strong thermo-responsive DS can substantially reduce the overall energy consumption of the entire ZLD process, as the brine volume to be treated by the energy intensive brine crystalliser can be reduced by more than 15 % when increasing the target brine concentration from 205 g/kg to 245 g/kg for the MBC.

One aspect of this comparison which has not been discussed so far is that the LSRRO and the conventional OARO process do not require any cooling water or heat transfer equipment, which conversely can significantly increase the cost of the FO and OARO MBC. Therefore, when operating with thermo-responsive DS, the OARO MBC outperforms the FO MBC in terms of a 31% lower specific cooling load (SCL) and a DSR temperature which is approximately 11C lower; both of these factors can reduce the cost of the heat transfer equipment and reduce the size of the reboilers, when powered by the same thermal source.

Another important consideration when choosing between purely pressure driven (LSRRO) and osmotically

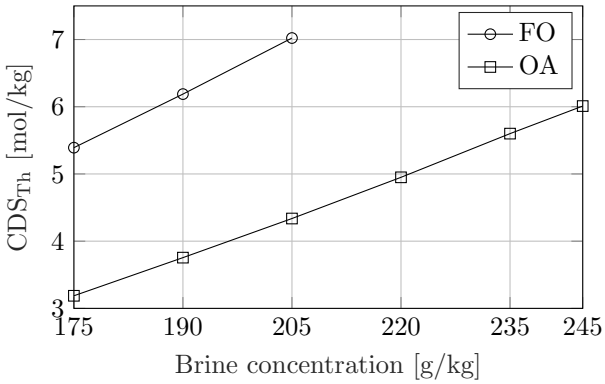

Figure 13: The required concentration of the thermo-responsive DS in the CDS stream CDS_{Th} with respect to the target brine concentration. The initial feed concentration is 35 g/kg NaCl.

driven processes (FO and OARO) is that the module design is, in general, more complex for the latter (Wang et al. 2020). Furthermore, it has also been highlighted by Wang et al. (2020) that operating at high hydraulic pressures while requiring thin membranes to mitigate ICP is a major technical limitation of the conventional OARO process. However, a new study by Chen et al. (2020) indicates that ICP may be less detrimental to OARO performance than previously thought. In the conventional OARO process, forward salt transport actually helps mitigate ICP and thus Chen et al. (2020) points out that the membrane's active layer properties (A and B) are important parameters that need to be considered for OARO optimisation. Furthermore, the membrane's S-value plays a less crucial role in OARO than in FO. This finding has important implications on the design of OARO membranes, and means that less dense membranes with thicker support layers may actually be ideal and allow for higher pressure operation to achieve high brine concentrations with conventional OARO processes. Choosing OARO with either a

non-responsive or a responsive DS therefore seems not only technically feasible, but also both options offer a significantly lower electrical energy consumption than LSRRO.

4 Conclusions

In this study, a numerical model is developed to simulate an OARO and an FO integrated ZLD process, whose design is based on the membrane brine concentrator. A direct parametric and techno-economic comparison is performed between both processes to highlight the benefits of combining OARO with a thermo-responsive DS and how OARO can alleviate several of the shortcomings of FO. Furthermore, the OARO and FO MBC are compared to the conventional OARO and the LSRRO process in order to identify which of these novel membrane-based ZLD processes is the superior technology.

The findings from this study can be summarised as follows:

- Extremely high brine concentrations of up to 245 g/kg can be achieved by the OARO MBC at technically feasible operating pressures (48.3 bar) and at reasonable draw solute concentrations (6 mol/kg on a carbon basis). This high brine concentration is not achievable by the FO MBC utilising the same thermo-responsive DS or by the conventional OARO system using a non-responsive DS.

- Utilising a thermo-responsive DS allows for the utilisation of low-cost thermal energy to drive the desalination process. The integration of LGWH can substantially reduce the required electrical energy consumption to levels below those achievable by LSRRO and by the conventional OARO process. However, one main disadvantage of utilising thermo-responsive draw solutes is that additional heat transfer equipment and cooling water are required, which is not the case for LSRRO and the conventional OARO process. These side effects can, however, be minimised by the OARO MBC, as the specific cooling load is reduced by 31 % in comparison to its FO counterpart.

- In comparison to FO, the high hydraulic pressure operation of OARO reduces the draw solute concentration required to achieve the same water flux and process recovery. This offers benefits, such as a lower susceptibility to ICP and a lower reverse solute flux, which in turn may confer additional advantages, such as allowing the removal of the energy intensive and costly brine stripper (DC1 in figure 2) from the process when combined with the development of more selective membranes or of draw solutes with a lower reverse transport rate.

- The UWC of the BVM process can be reduced by approximately 15.5 % by operating the MBC in OARO mode. Furthermore, OARO is more suited to LGWH integration than FO, as the reboilers of the OARO MBC can be operated at temperatures up to 12 C lower. LGWH integration is economically more sensible for high prevailing grid electricity costs, as the operational cost savings then outweigh the capital cost increase caused by the use of larger reboilers.

- With regards to membrane fouling, several uncertainties remain as to whether OARO or FO are more prone to membrane fouling, and to whether high pressure operation of the OARO membrane process is deleterious because of the deformation of the thin membrane. Fouling and membrane deformation have not been considered in this study and need to be addressed in future studies.

5 Acknowledgements

The authors would like to thank the University of Bahrain (in the Kingdom of Bahrain) for supporting and funding this research work.

References

Alameddine, I. & El-Fadel, M. (2007), 'Brine discharge from desalination plants: a modeling approach to an optimized outfall design', *Desalination* **214**(1-3), 241–260.

Arnal, J., Sancho, M., Iborra, I., Gozálvez, J., Santafé, A. & Lora, J. (2005), 'Concentration of brines from RO desalination plants by natural evaporation', *Desalination* **182**(1-3), 435–439.

Bacchin, P., Aimar, P. & Field, R. W. (2006), 'Critical and sustainable fluxes: Theory, experiments and applications', *Journal of Membrane Science* **281**(1), 42–69.

Bartholomew, T. V. & Mauter, M. S. (2019), 'Computational framework for modeling membrane processes without process and solution property simplifications', *Journal of Membrane Science* **573**, 682–693.

Bartholomew, T. V., Mey, L., Arena, J. T., Siefert, N. S. & Mauter, M. S. (2017), 'Osmotically assisted reverse osmosis for high salinity brine treatment', *Desalination* **421**, 3–11.

Bartholomew, T. V., Siefert, N. S. & Mauter, M. S. (2018), 'Cost Optimization of Osmotically Assisted Reverse Osmosis', *Environmental Science and Technology* .

Boo, C., Khalil, Y. F. & Elimelech, M. (2015), 'Performance evaluation of trimethylaminecarbon dioxide thermolytic draw solution for engineered osmosis', *Journal of Membrane Science* **473**, 302–309.

Bouma, A. T. & Lienhard, J. H. (2018), 'Split-feed counterflow reverse osmosis for brine concentration', *Desalination* **445**, 280–291.

Cai, Y. & Hu, X. M. (2016), 'A critical review on draw solutes development for forward osmosis', *Desalination* **391**, 16–29.

Cai, Y., Shen, W., Wei, J., Chong, T. H., Wang, R., Krantz, W. B., Fane, A. G. & Hu, X. (2015), 'Energy-efficient desalination by forward osmosis using responsive ionic liquid draw solutes', *Environmental Science: Water Research and Technology* **1**(3), 341–347.

Table 3: Comparison of the LSRRO, the standard OARO and the FO and OARO MBC with a thermo-responsive DS to concentrate a 35 g/kg saline stream to 205 g/kg (0.6 M to 4 M). The FO and OARO MBC are operated using a single RO pass and with the following parameters: $N/C = 2.4$, $Q_{MBC} = 5\,m^3/h$, $RR = 0.5$, $P_{RO1} = 80\,bar$, $Q_{RO} = 12\,m^3/h$.

		FO [a] (thermo-responsive DS)	OARO [a] (thermo-responsive DS)	LSRRO [b]	OARO [c] (non-responsive DS)
Total stages (+RO)		4	4	4	6
ΔP_{Max}	[bar]	1.0	48.3	70.0	68.0
CDS_{Th}	[mol/L]	7.0	4.3	-	-
$T_{Reb,DC1}$	[C]	97.2	86.1	-	-
$T_{Reb,DC2}$	[C]	91.5	80.3	-	-
SCL	$[MJ/m^3]$	351	242	-	-
W_{Eq}	$[kWh/m^3]$	11.1	9.3	5.14	3.9
SEEC	$[kWh/m^3]$	2.94	3.47	5.14	3.9

[a] This study
[b] Wang et al. (2020)
[c] Bouma & Lienhard (2018)

Campione, A., Gurreri, L., Ciofalo, M., Micale, G., Tamburini, A. & Cipollina, A. (2018), 'Electrodialysis for water desalination: A critical assessment of recent developments on process fundamentals, models and applications', *Desalination* **434**, 121–160.

Casas, S., Aladjem, C., Cortina, J. L., Larrotcha, E. & Cremades, L. V. (2012), 'Seawater Reverse Osmosis Brines as a New Salt Source for the Chlor-Alkali Industry: Integration of NaCl Concentration by Electrodialysis', *Solvent Extraction and Ion Exchange* **30**(4), 322–332.

Cengel, Y. A. & Boles, M. A. (2011), *Thermodynamics : an engineering approach*, 9th editio edn, McGraw-Hill.

Chekli, L., Phuntsho, S., Kim, J. E., Kim, J., Choi, J. Y., Choi, J.-S., Kim, S., Kim, J. H., Hong, S., Sohn, J. & Shon, H. (2016), 'A comprehensive review of hybrid forward osmosis systems: Performance, applications and future prospects', *Journal of Membrane Science* **497**, 430–449.

Chen, X., Boo, C. & Yip, N. Y. (2020), 'Transport and structural properties of osmotic membranes in high-salinity desalination using cascading osmotically mediated reverse osmosis', *Desalination* **479**, 114335.

Chen, X. & Yip, N. Y. (2018), 'Unlocking High-Salinity Desalination with Cascading Osmotically Mediated Reverse Osmosis: Energy and Operating Pressure Analysis', *Environmental Science & Technology* **52**(4), 2242–2250.

Claumann, C. A., Parisotto, I. G. B., Peruzzo, T., De Felice, V., Marangoni, C. & Machado, R. A. F. (2015), Modeling and Process Optimization: An Approach using Aspen Plus and Matlab in the Energy Integration Study of Distillation Columns, Technical report, AAIQ.

Coday, B. D., Xu, P., Beaudry, E. G., Herron, J., Lampi, K., Hancock, N. T. & Cath, T. Y. (2014), 'The sweet spot of forward osmosis: Treatment of produced water, drilling wastewater, and other complex and difficult liquid streams', *Desalination* **333**(1), 23–35.

Cengel, Y. A. & Ghajar, A. J. A. J. (2014), *Heat and Mass Transfer: Fundamentals and Applications*, 5 edn, Mc Graw Hill.

Darde, V., Maribo-Mogensen, B., van Well, W. J., Stenby, E. H. & Thomsen, K. (2012), 'Process simulation of CO 2 capture with aqueous ammonia using the Extended UNIQUAC model', *International Journal of Greenhouse Gas Control* .

Davenport, D. M., Deshmukh, A., Werber, J. R. & Elimelech, M. (2018), 'High-Pressure Reverse Osmosis for Energy-Efficient Hypersaline Brine Desalination: Current Status, Design Considerations, and Research Needs', *Environmental Science & Technology Letters* .

Dong, S., Heyda, J., Yuan, J. & Schalley, C. A. (2016), 'Lower critical solution temperature (LCST) phase behaviour of an ionic liquid and its control by supramolecular hostguest interactions', *Chemical Communications* **52**(51), 7970–7973.

DOW Water Solutions (2017), 'FILMTEC Reverse Osmosis Membranes: Technical Manual'.

Fontalvo Alzate, J. (2014), 'Using user models in Matlab® within the Aspen Plus® interface with an Excel® link', *Ingeniería e Investigación* **34**(2), 39–43.

Franken, A. C. M. (2009), 'Prevention and control of membrane fouling: Practical implications and examining recent innovations', *Membraan Applicatie Centrum Twente b.v.* .

Gingerich, D. B. & Mauter, M. S. (2015), 'Quantity, Quality, and Availability of Waste Heat from United States Thermal Power Generation', *Environmental Science and Technology* .

Hancock, N. T. & Cath, T. Y. (2009), 'Solute Coupled Diffusion in Osmotically Driven Membrane Processes', *Environmental Science & Technology* **43**(17), 6769–6775.

Jilvero, H., Normann, F., Andersson, K. & Johnsson, F. (2014), 'The Rate of CO2 Absorption in AmmoniaImplications on Absorber Design', *Industrial & Engineering Chemistry Research* **53**(16), 6750–6758.

Johnson, D. J., Suwaileh, W. A., Mohammed, A. W. & Hilal, N. (2018), 'Osmotic's potential: An overview of draw solutes for forward osmosis', *Desalination* **434**, 100–120.

Jones, E., Qadir, M., van Vliet, M. T., Smakhtin, V. & Kang, S.-m. (2019), 'The state of desalination and brine production: A global outlook', *Science of The Total Environment* **657**, 1343–1356.

Kim, J., Blandin, G., Phuntsho, S., Verliefde, A., Le-Clech, P. & Shon, H. (2017), 'Practical considerations for operability of an 8" spiral wound forward osmosis module: Hydrodynamics, fouling behaviour and cleaning strategy', *Desalination* **404**, 249–258.

Kim, J., Kim, D. I. & Hong, S. (2018), 'Analysis of an osmotically-enhanced dewatering process for the treatment of highly saline (waste)waters', *Journal of Membrane Science* **548**, 685–693.

Abbreviations

BVM	Brine volume minimisation
CapEx	Capital expenditures
CDS	Concentrated draw solution
CF	Capitalisation factor
DS	Draw solution
DDS	Diluted draw solution
DSR	Draw solute regeneration
ECP	External concentration polarisation
ERD	Energy recovery device
FO	Forward osmosis
GOR	Gained output ratio
HEX	Heat exchanger
HPRO	High-pressure reverse osmosis
ICP	Internal concentration polarisation
LGWH	Low-grade waste heat
MBC	Membrane brine concentrator
MCr	Membrane crystallisation
MD	Membrane distillation
MSRO	Multi-stage reverse osmosis
MVC	Mechanical vapour compression
N/C	Ammonia to carbon dioxide ratio
OARO	Osmotically assisted reverse osmosis
OpEx	Operational expenditures
RSF	Reverse solute flux
SCL	Specific cooling load
SEEC	Specific electrical energy consumption
STEC	Specific thermal energy consumption
TAC	Total annual cost
TDS	Total dissolved solids
TFC	Thin film composite
UWC	Unit water cost
WHO	World Health Organisation
WW	Wastewater
ZLD	Zero liquid discharge

Nomenclature

A	Water permeability coefficient, $L \cdot m^{-2} \cdot s^{-1} \cdot bar^{-1}$
B	Salt permeability coefficient, $L \cdot m^{-2} \cdot h^{-1}$
C_{BP}	Booster pump cost, \$
C_{CO2}	Carbon dioxide concentration, mol/kg
C_{Cond}	Condenser cost, \$
C_{DC}	Distillation column cost, \$
C_{DS}	Draw solute purchasing cost, \$
C_{ERD}	ERD cost, \$
C_{HEX}	HEX cost, \$
C_{HPP}	High-pressure pump cost, \$
C_{Mem}	Membrane unit cost, \$
C_{NaCl}	NaCl concentration, mol/kg
C_{NH3}	Ammonia concentration, mol/kg
C_{PV}	Pressure vessel unit cost, \$

Nomenclature

C_{Reb}	Reboiler unit cost, \$
$CapEx_{DSR}$	CapEx of the DSR system, \$
$CapEx_{Mem}$	CapEx of the membrane systems, \$
D	Diffusivity coefficient, m^2/s
F	Practical investment factor
$h_{fg,Steam}$	Enthalpy of vaporization, kJ/kg
$h_{g,Cond}$	Steam enthalpy in the condenser, kJ/kg
$h_{g,Steam}$	Enthalpy of the extracted steam, kJ/kg
J_S	Salt flux, $g \cdot m^{-2} \cdot h^{-1}$
J_W	Water flux, $L \cdot m^{-2} \cdot h^{-1}$
K	Mass transfer resistance, $m^2 \cdot h/L$
k_D	Mass transfer coefficient in draw stream, $L \cdot m^{-2} \cdot h^{-1}$
k_F	Mass transfer coefficient in feed stream, $L \cdot m^{-2} \cdot h^{-1}$
k_M	Mass transfer coefficient in the membrane, $L \cdot m^{-2} \cdot h^{-1}$
O_{Chem}	Chemical consumption cost, $\$/year$
O_{CW}	Cooling water cost, $\$/kWh$
O_{DS}	Draw solute replenishment cost, $\$/year$
O_{Elec}	Electricity cost, $\$/kWh$
O_{Mem}	Membrane replacement cost, $\$/year$
O_{ML}	Maintenance and labour cost, $\$/year$
$OpEx_{DSR}$	OpEx of the DSR system, $\$/year$
$OpEx_{Mem}$	OpEx of the membrane systems, $\$/year$
P_{Sat}	Saturation pressure, bar
P_D	Pressure of the draw solution, bar
P_F	Pressure of the feed solution, bar
P_{Low}	Low feed pressure, bar
Q_D	Draw flowrate, m^3/h
Q_F	Feed flowrate, m^3/h
Q_{MBC}	Feed flowrate of the MBC membrane modules, m^3/h
RR	Ratio between draw and feed flowrate
RSF_{MBC}	Reverse solute flux in the MBC membrane modules, g_{NH3}/kg
S	Structural parameter, m
S_1 to S_3	MBC membrane stages
S_{In}	Inlet salinity, g/L
T_{Reb}	Reboiler temperature, C
t_S	Support layer thickness, m
W_{Eq}	Equivalent work, kWh/m^3
ϵ	Porosity
η_{Tur}	Turbine efficiency
τ	Tortuosity
ΔP	Transmembrane pressure difference, bar
ΔP_{Max}	Maximum transmembrane pressure, bar
$\Delta\pi$	Osmotic pressure difference, bar
π_D	Osmotic pressure of draw solution, bar
π_F	Osmotic pressure of feed solution, bar

Kim, Y. C. & Park, S.-J. (2011), 'Experimental Study of a 4040 Spiral-Wound Forward-Osmosis Membrane Module', *Environmental Science & Technology* **45**(18), 7737–7745.

Lara, J., Osunsan, O. & Holtzapple, M. (2012), Advanced Mechanical Vapor-Compression Desalination System, *in*

M. Schorr, ed., 'Desalination, Trends and Technologies', IntechOpen, chapter 7.

Lee, J., Kook, S., Lee, C. & Kim, I. S. (2017), 'Effect of intermittent pressure-assisted forward osmosis (I-PAFO) on organic fouling', *Desalination* **419**, 60–69.

Loganathan, P., Naidu, G. & Vigneswaran, S. (2017), 'Mining valuable minerals from seawater: a critical review', *Environmental Science: Water Research & Technology* **3**(1), 37–53.

Lotfi, F., Chekli, L., Phuntsho, S., Hong, S., Choi, J. Y. & Shon, H. K. (2017), 'Understanding the possible underlying mechanisms for low fouling tendency of the forward osmosis and pressure assisted osmosis processes', *Desalination* **421**, 89–98.

Lu, Y. Y., Hu, Y. D., Zhang, X. L., Wu, L. Y. & Liu, Q. Z. (2007), 'Optimum design of reverse osmosis system under different feed concentration and product specification', *Journal of Membrane Science* .

Luo, H., Wang, Q., Zhang, T. C., Tao, T., Zhou, A., Chen, L. & Bie, X. (2014), 'A review on the recovery methods of draw solutes in forward osmosis', *Journal of Water Process Engineering* **4**, 212–223.

Luyben, W. L., ed. (2013), *Distillation Design and Control Using Aspen Simulation*, John Wiley & Sons, Inc., Hoboken, New Jersey.

McCutcheon, J. R., McGinnis, R. L. & Elimelech, M. (2005), 'A novel ammoniacarbon dioxide forward (direct) osmosis desalination process', *Desalination* **174**(1), 1–11.

McGinnis, R. L. & Elimelech, M. (2007), 'Energy requirements of ammoniacarbon dioxide forward osmosis desalination', *Desalination* **207**(1-3), 370–382.

McGinnis, R. L., Hancock, N. T., Nowosielski-Slepowron, M. S. & McGurgan, G. D. (2013), 'Pilot demonstration of the NH3/CO2 forward osmosis desalination process on high salinity brines', *Desalination* **312**, 67–74.

Mericq, J.-P., Laborie, S. & Cabassud, C. (2010), 'Vacuum membrane distillation of seawater reverse osmosis brines', *Water Research* **44**(18), 5260–5273.

Mezher, T., Fath, H., Abbas, Z. & Khaled, A. (2011), 'Techno-economic assessment and environmental impacts of desalination technologies', *Desalination* **266**(1), 263–273.

Miller, S., Shemer, H. & Semiat, R. (2015), 'Energy and environmental issues in desalination', *Desalination* **366**, 2–8.

Missimer, T. M. & Maliva, R. G. (2018), 'Environmental issues in seawater reverse osmosis desalination: Intakes and outfalls', *Desalination* **434**, 198–215.

Morillo, J., Usero, J., Rosado, D., El Bakouri, H., Riaza, A., Bernaola, F.-J., Bakouri, H. E., Riaza, A. & Bernaola, F.-J. (2014), 'Comparative study of brine management technologies for desalination plants', *Desalination* **336**, 32–49.

Nguyen, T.-T., Kook, S., Lee, C., Field, R. W. & Kim, I. S. (2019), 'Critical flux-based membrane fouling control of forward osmosis: Behavior, sustainability, and reversibility', *Journal of Membrane Science* **570-571**, 380–393.

Pendergast, M. M., Nowosielski-Slepowron, M. S. & Tracy, J. (2016), 'Going big with forward osmosis', *Desalination and Water Treatment* **57**(55), 26529–26538.

Petchers, N. (2012), *Combined heating, cooling and power handbook: Technologies and applications an integrated approach to energy resource optimization*, The Fairmont Press.

Peters, C. & Hankins, N. (2019), 'Osmotically assisted reverse osmosis (OARO): Five approaches to dewatering saline brines using pressure-driven membrane processes', *Desalination* .

Qin, M., Deshmukh, A., Epsztein, R., Patel, S. K., Owoseni, O. M., Walker, W. S. & Elimelech, M. (2019), 'Comparison of energy consumption in desalination by capacitive deionization and reverse osmosis', *Desalination* **455**, 100–114.

Reig, M., Casas, S., Aladjem, C., Valderrama, C., Gibert, O., Valero, F., Centeno, C. M., Larrotcha, E. & Cortina, J. L. (2014), 'Concentration of NaCl from seawater reverse osmosis brines for the chlor-alkali industry by electrodialysis', *Desalination* **342**, 107–117.

Roberts, D. A., Johnston, E. L. & Knott, N. A. (2010), 'Impacts of desalination plant discharges on the marine environment: A critical review of published studies', *Water Research* **44**(18), 5117–5128.

Ruiz Salmón, I. & Luis, P. (2018), 'Membrane crystallization via membrane distillation', *Chemical Engineering and Processing - Process Intensification* **123**, 258–271.

Sanmartino, J., Khayet, M., García-Payo, M., El-Bakouri, H. & Riaza, A. (2017), 'Treatment of reverse osmosis brine by direct contact membrane distillation: Chemical pretreatment approach', *Desalination* **420**, 79–90.

Shaffer, D. L., Werber, J. R., Jaramillo, H., Lin, S. & Elimelech, M. (2015), 'Forward osmosis: Where are we now?', *Desalination* **356**, 271–284.

Shon, H. K., Chekli, L., Phuntsho, S., Kim, J. & Cho, J. (2015), Draw Solutes in Forward Osmosis Processes, *in* 'Forward Osmosis', American Society of Civil Engineers, Reston, VA, pp. 85–113.

Siddiqui, F. A., She, Q., Fane, A. G. & Field, R. W. (2018), 'Exploring the differences between forward osmosis and reverse osmosis fouling', *Journal of Membrane Science* **565**, 241–253.

Straub, A. P., Yip, N. Y. & Elimelech, M. (2014), 'Raising the Bar: Increased Hydraulic Pressure Allows Unprecedented High Power Densities in Pressure-Retarded Osmosis', *Environmental Science & Technology Letters* **1**(1), 55–59.

Subramani, A. & Jacangelo, J. G. (2014), 'Treatment technologies for reverse osmosis concentrate volume minimization: A review', *Separation and Purification Technology* **122**, 472–489.

Tong, T. & Elimelech, M. (2016), 'The Global Rise of Zero Liquid Discharge for Wastewater Management: Drivers, Technologies, and Future Directions', *Environmental Science & Technology* **50**(13), 6846–6855.

Tow, E. W., Warsinger, D. M., Trueworthy, A. M., Swaminathan, J., Thiel, G. P., Zubair, S. M., Myerson, A. S. & Lienhard V, J. H. (2018), 'Comparison of fouling propensity between reverse osmosis, forward osmosis, and membrane distillation', *Journal of Membrane Science* **556**, 352–364.

Tsai, J.-H., Macedonio, F., Drioli, E., Giorno, L., Chou, C.-Y., Hu, F.-C., Li, C.-L., Chuang, C.-J. & Tung, K.-L. (2017), 'Membrane-based zero liquid discharge: Myth or reality?', *Journal of the Taiwan Institute of Chemical Engineers* **80**, 192–202.

Voutchkov, N. (2018), 'Energy use for membrane seawater desalination: Current status and trends', *Desalination* **431**, 2–14.

Wang, K. Y., Ong, R. C. & Chung, T.-S. (2010), 'Double-Skinned Forward Osmosis Membranes for Reducing Internal Concentration Polarization within the Porous Sublayer', *Industrial & Engineering Chemistry Research* **49**(10), 4824–4831.

Wang, P. (2016), *Smart Materials for Advanced Environmental Applications*, Smart Materials Series, The Royal Society of Chemistry.

Wang, Z., Deshmukh, A., Du, Y. & Elimelech, M. (2020), 'Minimal and zero liquid discharge with reverse osmosis using low-salt-rejection membranes', *Water Research* **170**, 115317.

Xiao, D., Li, W., Chou, S., Wang, R. & Tang, C. Y. (2012), 'A modeling investigation on optimizing the design of forward osmosis hollow fiber modules', *Journal of Membrane Science* **392-393**, 76–87.

Zeng, L.-m., Du, M.-y., Wang, X.-l., Zeng, L.-m., Du, M.-y. & Wang, X.-l. (2017), 'A Thermodynamical Approach for Evaluating Energy Consumption of the Forward Osmosis Process Using Various Draw Solutes', *Water* **9**(3), 189.

Zhou, X., Gingerich, D. B. & Mauter, M. S. (2015), 'Water Treatment Capacity of Forward-Osmosis Systems Utilizing Power-Plant Waste Heat', *Industrial & Engineering Chemistry Research* **54**(24), 6378–6389.